

# 1 A new inventory of High Mountain Asia surging glaciers derived from 2 multiple elevation datasets since the 1970s

3 Lei Guo<sup>1</sup>, Jia Li<sup>1</sup>, Amaury Dehecq<sup>2</sup>, Zhiwei Li<sup>1</sup>, Xin Li<sup>3</sup>, Jianjun Zhu<sup>1</sup>

4 <sup>1</sup>School of Geo-science and Info-physics, Central South University, Changsha, 410083, China.

5 <sup>2</sup>Univ. Grenoble Alpes, IRD, CNRS, Grenoble INP, IGE, Grenoble, 38000, France.

6 <sup>3</sup>Institute of Tibetan Plateau Research, Chinese Academy of Sciences, Beijing, 100101, China.

7

8 *Correspondence to:* Jia Li (lijia20050710@csu.edu.cn)

9 **Abstract.** Glacier surging is an unusual instability of ice flow and complete inventories of surging glaciers inventories are  
10 important for regional glacier mass balance studies and assessing glacier related hazards glacier dynamic studies. Glacier surge  
11 events in High Mountain Asia (HMA) are widely reported. However, the completeness of present inventories of HMA surging  
12 glaciers is constrained by the insufficient spatial and temporal coverage of glacier change observations, or by the limitations  
13 of the identification methods. In this paper study, we established a new inventory of HMA surging glaciers based on the glacier  
14 surface elevation changes and morphological changes over four decades. Four types kinds of elevation sources (the KH-9  
15 DEM, NASA DEM, COP30 DEM, and HMA DEM), three elevation change datasets, and long-term Landsat image series  
16 were utilized to assess the presence of typical surge features over two time periods (1970s-2000 and 2000-2020). A total of  
17 890 surging and 336 surge like probably or possibly surging glaciers were identified in HMA. Compared to the most recent  
18 previous inventory of surging glaciers inventories in HMA, our inventory incorporated 253 previously unidentified surging  
19 glaciers. The number and area of surging glaciers accounted for ~2.49% (excluding glaciers less smaller than 0.4 km<sup>2</sup>) and  
20 ~16.59% of the total glacier number and glacier area in HMA, respectively. Glacier surges were found in 21 of the 22  
21 subregions of HMA (except for the Dzhungarsky Alatau), however, the density of surging glaciers is highly uneven. Surging  
22 glaciers They are common in the northwest subregions (e.g., Pamir and Karakoram), but scarce in the peripheral subregions  
23 (e.g., Eastern Tien Shan, Eastern Himalaya, and Hengduan Shan). The inventory further confirmed that surge activity is more  
24 likely to occur for glaciers with a larger area, longer length, and wider elevation range. Among the glaciers with similar areas,  
25 the surging ones usually have steeper slopes s than the non-surging ones. Besides, we found a potential relationship between the  
26 surging glacier concentration and regional glacier mass balance. The subregions with slightly negative or positive mass balance  
27 hold large clusters of surging glaciers, while those with severe glacier mass loss hold very few surging glaciers. The inventory  
28 and elevation change products of identified surging glaciers are available at: <https://doi.org/10.5281/zenodo.7590838> (Guo et  
29 al., 2022).

30 **Key words:** High Mountain Asia, Surging glacier inventory, elevation change, KH-9, Digital Elevation Model (DEM)

## 31 1 Introduction

32 A surge is a glacier instability that translates into an abnormally fast flow over a period of a few months to years (Cogley et  
33 al., 2011). A surging glacier exhibits an active phase (surge) and a quiescent phase that may occur at quasi-periodic intervals  
34 (Jiskoot, 2011). During a glacier's surging phase. While a glacier enters into the surging states, a large volume of ice mass is  
35 transported downstream at a higher-than-average speed. In the quiescent phase, a glacier returns to a slow-moving state, and  
36 gradually regains mass in upper reeaches reaches.

37 Previous studies pointed out that the surge-type glaciers only represent ~1% of total glaciers (Jiskoot, 2011; Sevestre and Benn,  
38 2015). However, glacier surges are far more than an occasional behavior in some specific regions, such as the Alaska-Yukon  
39 (Clarke et al., 1986), Svalbard (Jiskoot et al., 2000; Farnsworth et al., 2016), and Karakoram-Pamir (Bhambri et al., 2017;

40 Goerlich et al., 2020; Guillet et al., 2022). Glaciers in these regions have experienced heterogeneous mass loss in the past  
41 decades (Hugonnet et al., 2021). How glacier surge activities impact the ~~glacier~~-regional mass balance needs further  
42 investigation, ~~and to facilitate this kind of study, the glacier surges needed to be found out first and requires to identify the~~  
43 ~~glacier surges firstly.~~

44 In recent years, substantial efforts have been made to understand the mechanisms of glacier surges, including the hydrological-  
45 control (Kamb, 1987; Fowler, 1987), thermal-control (Fowler et al., 2001; Murray et al., 2003), environmental factor (Hewitt,  
46 2007; Van Wyk de Vries et al., 2022), friction state (Thøgersen et al., 2019; Beaud et al., 2021), and the unified enthalpy  
47 balance model (Sevestre and Benn, 2015; Benn et al., 2019). ~~These theories require comprehensive validations by conducting~~  
48 ~~detailed analysis on various glacier samples.~~ To support ~~such studies, the accurate description of surging glacier distribution~~  
49 ~~is needed to provide samples for studying the internal dynamic process of surges~~ related investigations, ~~the distribution of~~  
50 ~~surging glaciers is needed as a starting point.~~ Besides, ~~glacier surge can induce several kinds of hazards, e.g., glacier lake~~  
51 ~~outbursts (GLOF) (Round et al., 2017; Steiner et al., 2018), mudslides (Muhammad et al., 2021), or ice collapse (Kääb et al.,~~  
52 ~~2018; Paul, 2019).~~ Such mountain hazards have been frequently reported in recent decades (An et al., 2021; Kääb et al., 2021).  
53 ~~A complete inventory of surging glaciers is a basis for the regional hazard assessment of glacier surges.~~

54 Generally, a surging glacier could exhibit either one or several drastic changes, including: extreme speed-up (by a factor of  
55 10~1000 compared to ~~normal conditions~~ ~~the usual flow of non-surging glaciers~~), distinct elevation change pattern, rapid  
56 terminus advance, and surface morphological changes (~~deformed~~ medial or looped moraines, crevasses, ~~shear margins~~, etc.)  
57 (Jiskoot, 2011). The identification of surging glaciers can be implemented based on the observation of the above changes, e.g.,  
58 glacier surface morphology (Clarke et al., 1986; Paul, 2015; Farnsworth et al., 2016), terminus position (Copland et al., 2011;  
59 Vale et al., 2021), ~~or~~ glacier motion (Quincey et al., 2011), ~~or morphological-related indicators (e.g., normalized backscatter~~  
60 ~~difference (Leclercq et al., 2021))~~. As for the ~~surge-type~~ glacier, which refers to ~~the a~~ glacier that possibly surged prior to the  
61 observation period, ~~are is~~ generally identified by ~~the~~ indirect morphological evidence (without observed changes) (Goerlich et  
62 al., 2020). The visual interpretation of glacier surface morphological changes is ~~less calculative~~ ~~easy to operate~~, but fraught  
63 with uncertainty due to the snow cover or the absence of supraglacial moraine ~~deformation~~ (Jacquemart and Cicoira, 2022).  
64 To recognize ~~abnormal-sudden~~ changes in glacier motion, a long-term flow velocity time series is ~~needed-needed~~ (Yasuda  
65 and Furuya, 2015; Round et al., 2017). Since the quiescent phase may last for decades and the image sources ~~for~~ estimating  
66 the flow velocity ~~is-are~~ limited, the ~~abnormal-strong~~ changes in glacier motion ~~are-prone to~~ ~~might~~ be missed. ~~By-In~~ contrast,  
67 the recognition of ~~abnormal-a specific~~ surface elevation changes ~~pattern~~ is ~~an-a more reliable~~ ~~effective~~ way to identify ~~the~~  
68 surging glaciers, ~~which has been confirmed by several glacier mass balance studies~~ ~~as it will be visible for many years before~~  
69 ~~and after a surge~~ (Bolch et al., 2017; Zhou et al., 2018). ~~Accordingly, as~~ its source datasets (DEMs) can satisfy the ~~requirement~~  
70 ~~required of spatial~~ ~~spatio~~-temporal coverage with comparatively fewer ~~acquisitions~~ ~~datasets~~. By combining observations of  
71 multiple features, the identification of surging glaciers could be more efficient and complete (Mukherjee et al., 2017; Goerlich  
72 et al., 2020; Guillet et al., 2022). However, when conducting such studies on a large spatial scale or a long temporal scale, one  
73 should select the least time-consuming but ~~most~~ effective identification method. In that case, it's ideal to take the long-term  
74 elevation change as ~~the a~~ ~~criteria~~ ~~criterion~~, ~~and to combine~~ ~~this information~~ with other observations ~~as complements~~ if possible  
75 (Guillet et al., 2022).

76 Except for the polar regions, High Mountain Asia (HMA) is the most densely glacierized region in the world. Within the HMA  
77 range, several subregions are famous for the concentration of surging glaciers as well as the ~~anomalous-differing~~ glacier mass  
78 balance (Hewitt, 2005; Gardelle et al., 2013; Farinotti et al., 2020). The inventories of surging or surge-like glaciers have been  
79 established for some subregions like the Karakoram (Bhambri et al., 2017), West-Kunlun (Yasuda and Furuya, 2015), Pamir  
80 ~~(Goerlich et al., 2020)~~, ~~(Goerlich et al., 2020)~~ and Tien Shan (Mukherjee et al., 2017; Zhou et al., 2021). Sevestre and Benn  
81 (2015) presented the first global ~~inventory of~~ ~~surging glaciers~~ ~~inventory~~ by reanalyzing historical reports from 1861 to 2013.  
82 However, it was compiled from various data sources (publications, reports, etc.) with inconsistent ~~spatial~~ ~~spatio~~-temporal



83 coverage, which makes it difficult to ensure accuracy and completeness. Vale et al. (2021) identified 137 surging glaciers  
84 across HMA by detecting surge-induced terminus change and morphological changes from Landsat images from 1987 to 2019.  
85 The number is obviously underestimated, because it is smaller than the numbers of previous subregional inventories (Bhambri  
86 et al., 2017; Goerlich et al., 2020), i.e. not all glaciers that surge do also advance. Guillet et al. (2022) presented a new surging  
87 glacier inventory of HMA by identifying multiple glacier change features. In total 666 surging glaciers were identified across  
88 HMA. However, the glacier change observation period is shorter than two decades (2000-2018), and therefore some surging  
89 glaciers with relatively long-repetition-revisit cycles may be missed.

90 In this study, we aimed to build a new inventory to include more surging glaciers within HMA based on glacier surface  
91 elevation changes observations over four decades. A workflow was developed to obtain the historical glacier surface elevation  
92 change from multiple datasets DEMs, including the KH-9 DEM (1970s), NASA\_DEM (2000), COP30 DSM-DEM (2011-2014),  
93 HMA 8m DEM (2002-late 2016), and previously published elevation change datasets. The preliminary identified surging  
94 glaciers in the new inventory were divided into three classes of confidence in surge detection. After that, the elevation change  
95 based inventory were-was further completed and corrected by the identification of morphological changes in a long-term time  
96 series of Landsat images (1986-2021). Based on the present inventory, the distribution and geometric characteristics of surging  
97 glaciers within HMA were statistically analyzed, in order to demonstrate their spatial heterogeneity and geometrical difference  
98 from the normal glaciers.

## 99 2 Study region

100 High Mountain Asia consists of the Qinghai-Tibet Plateau and the-its surrounding regions, including the Karakoram, Pamir,  
101 Himalayas, and Tien Shan. According to the updated Glacier Area Mapping for Discharge from the Asian Mountains  
102 (GAMDAM2) glacier inventory, HMA hosts 131819 glaciers, covering a total area of ~99817 km<sup>2</sup> (Sakai, 2019). The Hindu  
103 Kush Himalayan Monitoring and Assessment Programme (HiMAP) divided HMA into 22 subregions (Fig. 4) (Bolch et al.,  
104 2019). Different subregions are influenced by different climate regimes, such as the South Asia monsoon, the East Asia  
105 monsoons, and the westerlies (Bolch et al., 2012; Maussion et al., 2014). Glacier mass-balance-elevation changes across HMA  
106 were found to be heterogeneous in the past decades (Gardelle et al., 2013; Brun et al., 2017; Shean et al., 2020). In particular,  
107 glaciers in the Pamir-Karakoram-West Kunlun region had a-slightly positive or balance-close to zero mass budget changes  
108 (Hewitt, 2005; Zhou et al., 2017; Farinotti et al., 2020), while those in the Eastern Himalayas, Nyainqentanglha and Hengduan  
109 Shan mountain ranges experienced substantial ice loss (Maurer et al., 2019).

## 110 3 Datasets

### 111 3.1 Elevation Data

112 The NASA\_DEM is mainly reprocessed from the C-band SRTM (Shuttle Radar Topography Mission) images. Among the  
113 current global DEMs, the NASA\_DEM has the shortest source data acquisition period (~11/02/2000~22/02/2000) (Farr et al.,  
114 2007). Based on an improved production flow, the NASA\_DEM has a better performance than the earlier SRTM void-free  
115 product in most regions (Crippen et al., 2016). The NASA\_DEM was-employed-serves as the reference elevation source because  
116 its acquisition time, 2000, is suitable to divide the elevation change observations into before and after the 21<sup>st</sup> century with a  
117 moderate time span (one or two decades). Each tile of the product has an extent of 1°× 1° and a pixel spacing of 1 arc-second  
118 (see Fig. 1a). In total 313 tiles were downloaded from NASA LP DAAC  
119 ([https://e4ftl01.cr.usgs.gov/MEASURES/NASADEM\\_HGT.001/](https://e4ftl01.cr.usgs.gov/MEASURES/NASADEM_HGT.001/)).

120 Another global DEM we utilized is the newly released Copernicus DEM GLO-30-DGED (i.e., COP30 DEM). The COP30  
121 DEM was edited from the delicate WorldDEM™, which was generated based on the TanDEM-X mission. The global RMSE

122 of the COP30 DEM is  $\pm 1.68$  m (AIRBUS, 2020). Several studies have pointed out that this DEM is the most reliable open-  
123 access DEM to date (Purinton and Bookhagen, 2021; Guth and Geoffroy, 2021). The source images of the COP30 DEM were  
124 mostly acquired between 2011 and 2014, and therefore the COP30 DEM is suitable ~~to represent~~for representing the surface  
125 elevation in the 2010s. Like the NASA\_DEM, the COP30 DEM has a pixel spacing of 1 arc-second. Each tile of the product  
126 has an extent of  $1^\circ \times 1^\circ$ . In total 313 tiles were downloaded through ESA Panda ([https://panda.copernicus.eu/web/cds-](https://panda.copernicus.eu/web/cds-catalogue/panda)  
127 [catalogue/panda](https://panda.copernicus.eu/web/cds-catalogue/panda)).

128 The High Mountain Asia 8-meter DEM (HMA~~8m~~ DEM) was also utilized in this study. The HMA~~8m~~ DEM was generated  
129 from very high-resolution commercial optical satellite stereo images, including WorldView-1/2/3, GeoEye-1, and Quickbird-  
130 2 (Shean et al., 2020), through an automated photogrammetry workflow that is integrated with multiple error-control processes  
131 (Shean et al., 2016). This DEM was originally produced for the mass balance estimation of HMA glaciers, so it covered most  
132 of the glacierized regions in HMA. In total 3598 DEM tiles were downloaded from the National Snow and Ice Data Center  
133 ([https://nsidc.org/data/HMA\\_DEM8m\\_MOS/versions/1](https://nsidc.org/data/HMA_DEM8m_MOS/versions/1)). About 95% of them were acquired between 2010 and 2016 (Fig. 1b).  
134 Due to the data voids and inconsistent acquisition time, the HMA~~8m~~ DEM was taken as a supplementary elevation source to  
135 increase the observations in the 2010s.

136 The Hexagon KeyHole-9 (KH-9) imagery was acquired in the 1970s. It is one of the earliest near-global satellite stereo image  
137 sources. The KH-9 imagery is characterized by a spatial resolution of 6-9 m, a wide coverage (130 km x 260 km), and a 70%  
138 forward overlap (Surazakov and Aizen, 2010). Many studies have utilized this imagery to estimate historical glacier surface  
139 elevation (Holzer et al., 2015; Zhou et al., 2017; Maurer et al., 2019). The KH-9 DEMs used in this study were generated  
140 through the automated ASPy pipeline (Dehecq et al., 2020). The methodology, validated in the European Alps and Alaska,  
141 achieved a vertical accuracy of  $\sim 5$ m (68% confidence level). For more details on the method of KH-9 DEM generation, please  
142 refer to Dehecq et al. (2020). In total 238 DEMs with a resolution of 48 m were generated from the KH-9 images acquired  
143 between 1973 and 1980 (see Fig. 1c). The KH-9 DEMs were utilized to represent the glacier surface elevation in the 1970s  
144 (See Fig. 1c).

145 Several newly published elevation change datasets were also collected to include the most recent surges ~~as much as possible~~  
146 (Brun et al., 2017; Shean et al., 2020; Hugonnet et al., 2021). We mainly used the elevation change results presented by  
147 Hugonnet et al. (2021) to extend the observation period to 2020, which has a resolution of 100 m and a temporal interval of 5  
148 years. Through the inter-comparison of the multiple elevation change results, the gross errors or false signals in the elevation  
149 change patterns could be easily detected and removed.

## 150 3.2 Optical Satellite Images

151 In order to assist in the identification of surging glaciers, we also identified morphological changes associated with surges in  
152 multi-temporal optical satellite images. We mainly relied on the 1986-2021 Landsat imagery to capture ~~the glacier~~  
153 morphological changes. We acknowledge that due to the 30 m spatial resolution, not all details of a changed glacier surface  
154 are visible. We downloaded the false-colour composited Landsatlook images with 30m resolution (geo-referenced) that have  
155 good brightness contrast over snow/ice areas from the USGS ~~website~~ (<https://earthexplorer.usgs.gov>). The images were pre-  
156 selected to satisfy the requirement of cloud cover ( $<10\%$ ). In total, 7843 Landsatlook images in 148 frames were used (see Fig.  
157 1d). We also utilized the very high-resolution (VHR) images (Google/ESRI/Bing, etc.) as complements for surging feature  
158 identification. The fine resolution of these images allows us to visually check the possible morphological features caused by  
159 past surges.

## 160 3.3 Glacier inventory

161 In this study, we used the GAMDAM2 glacier inventory (Sakai, 2019) as a template for the inventory of surging glaciers  
162 ~~inventory~~, rather than the Randolph Glacier Inventory V6.0 (RGI6.0) (RGI Consortium, 2017). The GAMDAM glacier

163 inventory has included many small glaciers that are missed in RGI6.0, and provides a more accurate glacier extent by also  
164 excluding rock outcrop rocks, seasonal snow, and shaded areas (Nuimura et al., 2015). Since the GAMDAM2 inventory only  
165 contains the glacier polygon vectors, we calculated the geometric and topographic attributes for each glacier in a way similar  
166 to that of RGI6.0. The maximum glacier centreline was calculated through the Open Global Glacier Model (OGGM) (Maussion  
167 et al., 2019). The attributes were used to interpret the geometric characteristics of surging glaciers.

## 168 4 Methodology

### 169 4.1 Estimation of glacier surface elevation change

170 The four kinds of DEMs have different coordinate references, vertical references, and data formats. Firstly, all DEMs were  
171 converted to float GeoTiff format. For datasets with quality files (the NASA\_DEM and the COP30 DEM), the DEMs were  
172 preprocessed to mask out the pixels of low quality. The poor pixels of in the COP30 DEM tile were determined through the  
173 attached height error map (with values larger than 2.5 m) and water body map (with values not equal to zero). The NASA  
174 DEM was directly masked with the attached water mask file. Subsequently, the coordinate system, map projection, and vertical  
175 reference of all DEMs tiles were unified as the WGS84 coordinate system, HMA Albers Equal Area projection (Shean et al.,  
176 2020), and WGS84 ellipsoid. The glacier surface elevation changes during 2000-2010s were derived by subtracting the NASA  
177 DEM from the COP30 DEM and HMA DEM, and those during 1970s-2000 were derived by subtracting the KH-9 DEM  
178 from the NASA\_DEM.

179 An automated DEM differencing workflow for large-scale glacier surface elevation change estimation was developed based  
180 on the *demcoreg* package presented by Shean et al. (2019). The workflow integrated multiple DEM co-registration approaches,  
181 such as the polynomial fit of tilt error, and other adaptive outlier removal approaches that was-were operated based on the  
182 observations over stable regions. Hence, a mask that excluded the water bodies and glacierized regions was generated in  
183 advance. Before differencing, the two DEMs need to be co-registered, because a small geolocation shift can result in  
184 considerable elevation change errors in high-mountain regions. The efficient analytical DEM co-registration method presented  
185 by Nuth and Kääb (2011) was used to eliminate the relative geolocation shift (horizontal and vertical) between DEMs. This  
186 method assumes the geolocation shift vectors of all DEM pixels are identical. However, for the global DEM products like the  
187 NASA\_DEM and the COP30 DEM, a DEM tile was usually mosaiced-merged from multiple DEM patches, and the geolocation  
188 shift vectors at different parts of the DEM tile may be different. In view of this problem, we developed a block-wise version  
189 of the analytical DEM co-registration method to reduce the impacts of geolocation accuracy anisotropy of a DEM tile. Each  
190 DEM tile was divided into  $m \times n$  blocks, and the DEM shifts were estimated for each block. Then, the  $m \times n$  groups of shift  
191 parameters were merged into one group of shift parameters through a cubic interpolation. Technically, the estimated shift  
192 parameters become increasingly representative as the block size decreases. However, the fitting of shift parameters requires a  
193 certain number of samples. The final block size was set to  $300 \times 300$  pixels to reach the best balance between the  
194 representativeness and estimation accuracy of the shift parameters. Besides, we found that the block-wise co-registration  
195 method could result in wrong fitting of shift parameters over flat regions. To deal with this, a threshold of mean slope ( $10^\circ$ )  
196 was set to classify the DEMs into the flat and the hilly categories, and the original global co-registration method (Nuth and  
197 Kääb, 2011) was applied to the flat ones.

198 Due to the residual orbital error of satellite images, the elevation difference maps often showed planimetric trends. This type  
199 of systematic error was fitted as a universal surface trend using a quadratic polynomial model based on the observations in  
200 stable regions, and then was removed from the elevation difference tile (Li et al., 2017). Besides, due to the jitter of the SAR  
201 antenna and optical mapping camera, the elevation difference maps often showed stripes (i.e., band-like artifacts) (Yamazaki  
202 et al., 2017). To eliminate the stripes, the elevation difference map was converted to the frequency domain through the a Fast-  
203 Fourier-Transform method. Since the cyclic values have a high frequency in the power spectral density map, a threshold of

204 frequency was set to separate the stripes components from the normal elevation differences. The de-stripping was completed  
205 after the backward transformation. Finally, the outliers of elevation difference maps were reduced through the 3-sigma  
206 threshold ~~criteria~~criterion.  
207 The radar penetration into glacier surface can result in biases of elevation change estimation, which could be several to dozens  
208 of meters, and potentially ~~can lead to the false~~ positive identification values. We adopted a two-step procedure to reduce the  
209 radar penetration bias in the final elevation change results. First, we used the DEM differencing workflow mentioned above  
210 to subtract the NASA\_DEM from the SRTM-X DEM. The elevation differences over glacierized area were regarded as the  
211 penetration difference between X-bands and C-bands. Secondly, we fitted a 3<sup>rd</sup> polynomial function between the glacial dH  
212 and altitude, which was deemed as the penetration depth – altitude relationship. Then, the radar penetration biases were  
213 removed from the COP30 DEM related results by taking the glacier elevation as input for the function. For the dH results  
214 calculated by differencing the NASA\_DEM and optical DEMs (e.g. the HMA~~8m~~ and KH-9 DEM), the penetration difference  
215 of X- and C- bands was multiplied by 2 to represent the absolute penetration depth of C-band (Abdel Jaber et al., 2019; Fan et  
216 al., 2022) and then removed from the related results.  
217 Finally, three elevation change maps were calculated: the COP30 DEM – NASA\_DEM, the HMA~~8m~~ DEM – NASA\_DEM,  
218 and the NASA\_DEM – KH-9 DEM. The first two elevation change maps were combined with the three elevation change  
219 datasets for surging glacier identification during the period 2000-2020, and the last one during the period 1970s-2000. In total,  
220 our elevation change observations covered ~92% of the total glacier area within HMA in 2000-2020, and ~77% in 1970s-2000.  
221 Gaps in observations were mainly due to: 1) data voids and incomplete coverage of the original DEMs tile, which was the  
222 main cause for the KH-9 DEMs and HMA~~8m~~ DEM related results; 2) gross error removal during the elevation change  
223 calculations, which led to the scattered holes in the COP30 DEM related results.

#### 224 **4.23 Surging glacier identification**

225 The identification of surging glaciers in this study ~~were was~~ divided into three steps. First, we generated a raw inventory of  
226 surging glaciers through the qualitative interpretation of multi-temporal elevation changes. Then, the visual identification of  
227 morphological changes was carried out for the identified surging and surge-like glaciers. This procedure can further confirm  
228 the surges or correct the ~~false~~ identifications based on glacier elevation changes (Guillet et al., 2022). The identified results  
229 were re-checked by careful inspection on VHR images, and by comparing with ~~existed~~existing surging glacier inventory. Also,  
230 the surging tributaries were separated from the non-surging glacier trunk at this step.

##### 231 **4.23.1 Identification through elevation changes**

232 In general, a typical glacier surge cycle can be divided into three phases (Jiskoot, 2011): 1) the build-up phase, characterized  
233 by remarkable thickening in the upper reaches; 2) the active phase, characterized by remarkable thinning in the upper reaches  
234 and thickening in the lower reaches; 3) the post-surge phase, characterized by strong down-wasting in the lower reaches. The  
235 classical method of identifying surging glaciers is to recognize the combination of marked upper thinning and lower thickening  
236 in the longitudinal direction. However, to distinguish the surging glaciers in the build-up or post-surge phase, careful  
237 comparison with surrounding glaciers is required, which is difficult to be carried out with a mathematical index. In this study,  
238 we established a three-class indicator to distinguish the surge possibility through the visual interpretation of glacier elevation  
239 change patterns:

240 I) “verified”:

- 241 - a) obvious thickening in lower reaches (e.g. +30 m);
- 242 - b) contrasting upper-thinning (e.g. +20 m) and lower-thickening (e.g. +20 m);
- 243 - c) contrasting upper-thickening (e.g. +20 m) and lower-thinning (e.g. -30 m);

- d) severe thinning in the lower reaches (two times stronger than that of the normal glaciers, or comparable to the ablation of adjacent “verified” surging glaciers);

II) “probable”:

- a) moderate upper thinning (e.g. -15m) and lower thickening (e.g. +15m);

- b) only moderate thickening in the middle reaches (e.g. +15m);

III) “possible”:

- a) only moderate thickening at the terminus (e.g. +15m);

- b) only strong thinning in the lower reaches (one time stronger than adjacent normal glaciers).

Note that, the specific values of elevation change mentioned above were for information only. Because of the diversity in the regional elevation change patterns under different climate or topographic conditions, the thresholds may vary spatially.

The identification of surging glaciers was conducted separately in the two observation periods (1970s-2000 and 2000-2020).

The sub-inventory covering the period 1970s-2000 was generated based on the dH results of the NASA DEM – KH-9 DEM.

For the sub-inventory covering the period 2000-2020, its dH datasets contain the COP30 DEM – NASADEM, the HMA8m

DEM – NASADEM, and three previously published elevation change datasets (Brun et al., 2017; Shean et al., 2020; Hugonnet

et al., 2021). Within each observation period, each glacier will be labeled with its possibility level of surging and elevation

change pattern in the attribute table. For example, the label of “I-c” means this glacier was classified as a “verified” surging

glaciers because contrasting upper-thickening and lower-thinning patterns were observed in the corresponding period. Figure

2 shows an example of surging glacier identification result.

#### 4.32.2 Identification through morphological changes

Long-term Landsat images (acquired between 1986 and 2021) were utilized to investigate the morphological changes of the

three types of potential surging glaciers identified from elevation change. With each Landsat image acquisition frame, all

Landsatlook images of different dates (acquired from 1986 to 2021) were merged into an animated time-series image. Based

on the animated image, we are able to easily identify the morphological changes. Due to the moderate resolution of Landsat

images, only three types of feature changes were utilized as criteria for identifying glacier surges: terminus position change,

looped moraine changes, and medial moraine changes. Similarly, we assigned a two-level index to each morphological change

to indicate our confidence at the identification, which was defined as follows:

1) terminus advance:

I-I): obvious terminus advancing (e.g. over 500 m);

II): small-slight terminus advancing (e.g. -0~500 m);

2) looped/medial moraine change:

I-I): fast formation/vanishment of the looped moraine, or obvious distortion of the medial moraine;

II-II): slow formation or vanishment of the looped moraine, or slight shape changes of existed-existing looped moraine, or slight distortion of the medial moraine.

Each of the three kinds of morphological changes were individually qualified and labeled in the attribute table.

#### 4.32.3 Generation of surging glacier inventory

Through the above identification steps, in total five indicators were compiled to describe the changes of possible surging

glaciers. The two sub-inventories of dH identified results were merged firstly following the principle of possibility, i.e., if a

glacier was identified as a surging glacier in both periods but associated with different indicators, its indicator in the final

inventory was taken from the indicator having a higher possibility. The possibility of indicators follows the order: “verified” >

“probable” > “possible”. For example, a glacier was identified as a “verified” surging glacier in the period 1970s-2000, and

was identified as a “probable” surging glacier in the period 2000-2010s, then it was qualified as a “verified” surging glacier.



285 After that, the merged dH indicators were further compared with the morphological indicators to determine the final indicator  
286 of surge possibility. The “probable” or “possible” class was changed to a class with higher possibility (e.g., from “probable”  
287 to “verified”) only if an “I” kind of morphological change was found.

288 We think the advancing glaciers usually have such features: 1) only thickened in a small area at the terminus, without  
289 contrasting upper thinning; 2) the advancing distance is relatively short (Lv et al., 2019, 2020; Goerlich et al., 2020). These  
290 features are corresponding to the “III-a” type of elevation change, and the “II” type of terminus advance. Therefore, if a glacier  
291 only shows these two kinds of changes, it will be qualified as an advancing glacier, rather than a surging glacier.

292 For glacier complexes in which a tributary surged but the main trunk did not show any features of a surge, such as the Biafo  
293 glacier, Fedchenko Glacier, and Panmah Glacier (Hewitt, 2007; Goerlich et al., 2020; Bhambri et al., 2022), it’s necessary to  
294 separate the surging tributary from the trunk. A tributary will be considered as an individual surging glacier if it has the  
295 following features. Firstly, the transition of contrasting elevation change is located in this tributary. Secondly, the mass  
296 contributed by this tributary to the glacier trunk is relatively small. Then we manually edited the outline to separate the tributary  
297 from the glacier complex. This kind of surges was also marked by the attribute of “trib\_surge”.

298 In the final step, we inspected the identified surging glaciers on VHR imagery. The inspection aimed to remove the wrong  
299 identification due to some false signals, such as the severe lower-thinning in a lake-terminating glacier and remarkable surface  
300 heightening caused by nearby landslides. We also refined our inventory after careful comparison with inventories presented  
301 by Guillet et al. (2022), Goerlich et al. (2020), and Bhambri et al. (2017).

## 302 5 Results

### 303 5.1 Identified surging glaciers

304 A total of 1226 surge-related glaciers across the HMA were identified based on the elevation changes and morphological  
305 changes. The identified surge-related glaciers consisted of 890 ‘verified’ surging ones, 208 ‘probable’ ones, and 128 ‘possible’  
306 ones. A total of 175 surging tributaries were identified in 86 glacier complexes. When merging the identification results of the  
307 two periods, we found that a considerable proportion of identified surging glaciers were simultaneously recognized in ~~two~~  
308 both periods. This makes our inventory more reliable, since a surging glacier could exhibit different kinds of changes in  
309 different periods. For example, 26 probable and 51 possible surging glaciers identified during 2000-2020 turned out to be  
310 “verified” surging glaciers during 1970s-2000. Meanwhile, 60 “probable” and 21 “possible” surging glaciers identified during  
311 1970s-2000 turned out to be ‘verified’ surging glaciers during 2000-2020. Thanks to ~~an~~the almost complete coverage of ~~the~~  
312 elevation change observations, we were able to classify almost all glaciers in HMA. Table 1 shows the number of surging  
313 glaciers identified from two periods of elevation changes and morphological changes. Due to the incomplete coverage of KH-  
314 9 DEMs, 103 identified surging glaciers have no observations during the period 1970s-2000. The data voids in KH-9 DEMs  
315 may be one of the reasons why and data voids of KH-9 DEMs, fewer surging glaciers were surging glaciers identified were  
316 identified during the in this period 1970s-2000. In the following text, ~~the~~ “probable” and “possible” classes were deemed as  
317 surge-like glaciers. ~~To avoid confusion, and~~ only the “verified” surging glaciers were used for analysis and comparison  
318 throughout the rest of this study.

### 319 5.2 Distribution of surging glaciers

320 Surging glaciers were identified in 21 subregions of HMA (except for the Dzhungarsky Alatau), however, the density of  
321 identified surging glaciers is far from even (Fig. 3). Glacier surges are common in the northwest regions, sporadic in the inner  
322 regions, and scarce in the peripheral regions. Figure 4 and Table 2 show the ratios of surging glacier number and area in each  
323 subregion. Considering the area of the smallest identified surging glacier is 0.42 km<sup>2</sup>, we only took the glaciers larger than  
324 0.40 km<sup>2</sup> in the glacier number related ratio. When conducting statistical analysis, the surge-like glaciers were excluded from  
325 the dataset, and a surging tributary was regarded as an individual glacier. The number (890) and area (16556.42 km<sup>2</sup>) of

326 identified surging glaciers accounted for ~2.49% and ~16.59% of the total glacier number and glacier area in HMA,  
327 respectively.

328 Among the 22 subregions, the Karakoram is the largest cluster of surging glaciers. In total 354 surging and 128 surge-like  
329 glaciers were identified in the Karakoram. The number and area of verified surging glaciers in the Karakoram accounted for  
330 39.80% and 47.90% of the total identified surging glaciers within HMA. We found more than half of the tributary surges (101)  
331 occurred in the Karakoram, where large glaciers are much more developed than in other regions. In the Karakoram, although  
332 surging glaciers have only accounted for 8.59% of the total glacier number, their area occupied 39.48% of the total glacierized  
333 area. The Pamirs, composed of the Eastern Pamir, Western Pamir, and Pamir Alay, hosts 249 surging glaciers and 128 surge-  
334 like glaciers. About 27.74% of the glacier area in the Eastern and Western Pamir belongs to surging glaciers. We also found  
335 28 surging tributaries in 15 glacier complexes in the Pamirs. Surging glaciers are also common in the Western Kunlun. In total  
336 82 surging and 47 surge-like glaciers were identified in the West Kunlun, and the area of surging glaciers accounted for 30.48%  
337 of the total glacier area. The Central Tien Shan has the fourth-fourth-largest surging glacier area. In total 59 surging glaciers  
338 were identified in the Central Tien Shan, which covered 12.93% of the total glacier area. The Karakoram, Pamirs, West Kunlun,  
339 and Central Tien Shan host ~83% of the surging glaciers across HMA. Figure 5 shows the distribution of identified surging  
340 and surge-like glaciers in these four regions.

341 Within interior HMA subregions (including the Tibetan Interior Mountains, Eastern Kunlun Shan, and Tanggula Shan), the  
342 number of identified surging glaciers represents less than 2% of the total but the area accounted for nearly 15% of the total  
343 glacial-glacier area. Surging glaciers in these regions are generally gathered in a few watersheds. Similar localized surging  
344 glacier clusters were also found in the Nyainqentanglha, Northern, and Western Tien Shan, and Central Himalaya, but the  
345 corresponding area ratios are much lower. In these regions, our inventory covered dozens of surging glaciers, which were  
346 rarely reported before. Figure 6 shows some samples of identified surging glaciers in these regions.

### 347 5.3 Geometric characteristics of surging glaciers

348 In this part, only the surging glaciers and non-surging- glaciers are taken for analysis. The surge-like glaciers are not included.  
349 All glacier samples in the surging and non-surging classes are larger than 0.40 km<sup>2</sup>.

350 We divided all glaciers into 9 classes according to their area, and calculated the ratios of surging glacier number and area in  
351 each class. As shown in Figure 7 and Table 3, surging glaciers were found in all classes. Both the ratios of surging glacier area  
352 and number became increasingly high as the glacier size increased, except for the last class. Surging glaciers with an area of  
353 1~50 km<sup>2</sup> occupies-occupy 82% of all surging glaciers. For the three classes in which glaciers are larger than 50 km<sup>2</sup>, the ratios  
354 of surging glaciers area and number were about 52% and 54%, respectively. In particular, 2 of 6 very large glaciers (the Siachen  
355 glacier and the Hispar glacier) surged during our observation periods.

356 When comparing the geometric characteristics of the surging glaciers and non-surging glaciers, we selected samples in the  
357 following way: for each surging glacier, we selected 10 non-surging glacier samples that have the closest area; and then we  
358 randomly sampled 3 out of the 10 selected non-surging glaciers. This is to minimize the discrepancy resulted from the sample  
359 differences. There are two reasons for doing so. First, the gap between the sample numbers is huge (~35000 non-surging vs.  
360 890 surging). Second, a high proportion of non-surging glaciers are very small glaciers. The final selected 890×3 non-surging  
361 glaciers formed the reference group.

362 We first analysed-analyzed the distribution of surging glacier number and area in eight orientations. As shown in Fig. 8, both  
363 the number and area of glaciers facing the north are the largest, and then followed by those facing the northwest and northeast.  
364 The distribution of the glacier orientation in the reference group were-was different than-from that of the non-surging glaciers,  
365 which confirmed the statistical analysis would be affected by sample differences. The number of surging glaciers facing the  
366 north accounted for ~30.1% of the total surging glacier number, and their area accounted for ~27.8% of all surging glacier  
367 area. The number and area ratios of surging glaciers facing the north are obviously higher than that of the non-surging glaciers

368 facing ~~the~~north, while the number and area ratios of surging glaciers facing ~~the~~northwest are obviously lower than that of the  
369 non-surging glaciers facing ~~the~~northwest. Meanwhile, the area ratio of surging glaciers facing ~~the~~northeast is considerable  
370 considerably higher than the number ratio, but for surging glaciers facing ~~the~~northwest and southwest, the situation is opposite.  
371 Figure 9 illustrates the comparisons between the basic geometric properties of surging and non-surging glaciers. The sampling  
372 strategy mentioned above was also utilized here. If we directly compare the surging glaciers with all non-surging glaciers, we  
373 will find that surging glaciers generally have a larger area, wider elevation range (i.e., the highest glacier surface elevation  
374 minus the lowest), and longer flow\_line (Fig 9a-c). Taking the median values as the candidates, the quantitative comparisons  
375 are 7.3 km<sup>2</sup> (surging) vs. 0.87 km<sup>2</sup> (non-surging) for glacier area, 1534 m vs. 642 m for elevation range, and 6695 m vs. 1854  
376 m for maximum glacier length, respectively. In terms of mean surface slope and median elevation, the values of the surging  
377 glaciers are less spread out than the non-surging glaciers. However, the median values of the two kinds of glaciers are very  
378 close (see Figures 9d and 9e). If we took the non-surging glaciers in the reference group for comparisons, the discrepancies ~~of~~  
379 between the two kinds of groups on these geometric properties became much more different. As shown in Figure 9a, the similar  
380 boxplots of the reference group and surging glacier samples proved that our sampling strategy has successfully re-organized  
381 the non-surging glacier samples for comparisons. The gaps between the surging and non-surging glaciers (reference group) in  
382 the glacier area (7.3 km<sup>2</sup> vs. 7.0 km<sup>2</sup>), elevation range (1534 m vs. 1180 m), and glacier length (6695 m vs. 5560 m), are much  
383 smaller. More importantly, the mean slope of the glaciers in the reference group becomes smaller than that of the surging  
384 glaciers.

385 The correlation between different glacier geometric properties was ~~analysed-analyzed~~ through the bivariate scatterplots (see  
386 Figure 10). Among the glacier area, glacier length, and glacier surface elevation range, any two of them have an apparent  
387 positive correlation. The glacier mean slope has a moderate correlation with ~~the~~glacier area, ~~glacier~~length, and ~~glacier~~  
388 elevation range as they are auto-correlated. By contrast, ~~the~~glacier median elevation has little correlation with ~~glacier area,~~  
389 ~~glacier length, glacier elevation range~~these parameters, and ~~glacier mean slope~~. The correlation of any two geometric properties  
390 makes little difference between surging and non-surging glaciers.

## 391 **6 Discussion**

### 392 **6.1 Uncertainty analysis**

393 The reliability of surging glacier identification is directly related to the accuracy of glacier surface elevation change. Assuming  
394 the uncertainties in surface elevation change are similar over glacierized areas and stable areas, we evaluated the glacier  
395 elevation change uncertainties based on elevation change observations in stable areas, whose true values are zeros. Meanwhile,  
396 the uncertainties in the radar penetration calculation were also considered through the error propagation law. The normalized  
397 median absolute deviation (NMAD) is less sensitive to outliers and can be deemed as an alternative better proxy of uncertainty  
398 in dH ~~to~~than the standard deviation (Höhle and Höhle, 2009). Hence, the NMAD was used to denote the uncertainty of  
399 individual glacier surface elevation change tile (Li et al., 2017). Figure 11 shows the NMAD of elevation change observations  
400 in stable areas within each DEM differencing tiles, which were used for the co-registration and biases removal during the  
401 glacier elevation change estimation. Due to large distortions in the KH-9 images, the NASADEM ~~—~~ KH-9 DEM results had  
402 the highest uncertainties. Benefiting from the advantages of bistatic SAR image pairs, the COP30 DEM has high quality, and  
403 the COP30 DEM related results had the lowest uncertainties. The HMA~~8m~~ DEM related results had moderate uncertainties.  
404 The average NMAD of all DEM differencing tiles was smaller than 5 m. ~~The~~significant elevation errors usually occurred in  
405 ~~the~~highly rugged regions such as crests and horns. The terrain of glacier surface is relatively gentle, and therefore the  
406 uncertainties of glacier surface elevation changes should be lower than the estimated values over the area where surges occur.  
407 The ~~top-head~~ of glaciers usually includes very steep faces and ~~have~~has a lot of uncertainties, but it does not matter too much  
408 for this study. In general, the uncertainties of our elevation change results are well-controlled. Compared with the typical

409 surface elevation change resulting from a glacier surge (tens to hundreds of meters), the magnitudes of uncertainties are very  
410 small.

411 Similar to previous studies (Sevestre and Benn, 2015; Goerlich et al., 2020), the surging glacier identification in this study  
412 was completed through a manual qualitative interpretation. It's difficult to provide a quantitative index to represent the  
413 uncertainty of surge identification. However, the four-class indicator of surge likelihood could aid that ~~in~~to a degree.

## 414 6.2 Characteristics of surging glaciers

415 The direct comparisons between geometric characteristics of surging and non-surging glaciers manifest that surge activity is  
416 more likely to occur in the glacier with a larger area, wider elevation range, and longer length (Fig. 9). Previous studies also  
417 reported this phenomenon (Barrand and Murray, 2006; Jiskoot, 2011; Sevestre and Benn, 2015; Mukherjee et al., 2017; Guillet  
418 et al., 2022). Larger area, wider elevation range, and longer length mean a larger glacier scale and more mass storage. Surge  
419 is a self-balancing process of a glacier to regulate its internal instability of thermal or hydrologic conditions which needs  
420 enough mass storage. In this case, about 97% of the surging glacier has an area larger than 1 km<sup>2</sup>. For glaciers larger than 10  
421 km<sup>2</sup>, surge becomes a quite common behavior (with a number ratio higher than 20%), rather than an accidental behavior (see  
422 Fig.7).

423 In terms of mean surface slope, we could not observe a statistically significant difference in the median value of the surging  
424 and non-surging glaciers, although the surging glaciers have a more concentrated value range (Fig 9d and Figure 10, 3<sup>rd</sup> row,  
425 1<sup>st</sup> column). After minimizing this kind of bias, we observed an obviously higher mean slope of surging glaciers in the  
426 comparison with the reference group. Several studies have demonstrated that the surging glacier tends to have a shallower  
427 slope (Jiskoot et al., 2000; Guillet et al., 2022). However, here we reasonably argue that this rule was concluded from an  
428 unbalanced comparison, as non-surging glaciers have a higher proportion of small glaciers than surging glaciers. Meanwhile,  
429 the inverse relationship between the glacier slope and length (Clarke, 1991; Sevestre and Benn, 2015) may not apply to very  
430 small glaciers (i.e. smaller than 1 km<sup>2</sup>). As shown in Fig. 9d and Fig. 10, among the non-surging glaciers, the small ones  
431 occupy a high proportion and their mean slope presents strong variability. Regarding this, we can conclude that steeper glaciers  
432 are more likely to surge when the comparison is restricted to similar areas. As for the glacier median elevation, since it is  
433 almost irrelevant to the glacier area, glacier length, glacier elevation range, and glacier mean slope (see Fig. 10), it can be  
434 deemed as an irregular glacier index. However, among glaciers that have similar areas, steeper glaciers generally have a lower  
435 median elevation. That's why the median elevation of surging glaciers is slightly smaller than that of non-surging glaciers (Fig.  
436 9e).

437 These comparisons could now lead to a conclusion as follows: the surging glaciers are generally longer, and have a larger  
438 elevation range than non-surging glaciers, since they have more mass storage. However, when glaciers are similar in area, a  
439 steeper surface slope is more likely to lead to surge.

440 Besides, our results highlights that the ratio distribution of surging glaciers in eight aspects ~~are~~is slightly different from that  
441 of non-surging glaciers (see Fig. 8~~)~~). Overall, the ratio of surging glaciers is relatively higher than the non-surging glaciers  
442 in the north and northeast directions, but lower in the northwest direction. It is generally known that glaciers facing ~~the~~the  
443 are more developed in HMA. Due to the orientation of the mountains, most of the large glaciers flow toward ~~the north and north~~  
444 and northeast. Besides, the area-to-number ratio of surging glaciers is much larger than non-surging glaciers in the northeast  
445 orientation, but smaller in the northwest orientation. This is true for the Karakoram, Pamirs, and West Kunlun Shan, the three  
446 largest clusters of surging glaciers, ~~indicates~~indicating that large northeast-facing glaciers ~~has~~have a higher ~~possibility~~chance  
447 to be surging glaciers. Accordingly, the surging glaciers facing ~~the~~the north and northeast have ~~higher~~a higher area ratio than that  
448 facing the northwest.

449 The spatial distribution of surging glaciers in HMA presents a strong heterogeneity. About 83% of identified surging glaciers  
450 were located in the northwest region including the Central Tien Shan, Pamirs, Karakoram, and West Kunlun, and their area

451 occupied about 87% of the total identified surging glacier area (see Fig. 4 and Table 2). As discussed above, larger glaciers  
452 are more likely to surge. The northwest regions generally hold more large glaciers, and therefore hold more surging glaciers.  
453 In other subregions, large glaciers are usually concentrated in some great ice fields, such as the Geladandong, Puruogangri,  
454 and Xinqingfeng. Accordingly, surging glaciers in these subregions are usually clustered in several watersheds.  
455 Several studies have pointed out that glacier surge activities have little impact on the glacier mass balance (Gardelle et al.,  
456 2013; Bolch et al., 2017; Guillet et al., 2022). However, glacier mass balance may also affect the occurrence of glacier surges.  
457 Copland et al. (2011) concluded that the increase of glacier surges in the Karakoram could be related to the positive mass  
458 budget. The accumulated ice mass would accelerate a glacier to surge (Eisen et al., 2005; Kochtitzky et al., 2020), and the  
459 significant mass loss could prevent or postpone the surge in return (Dowdeswell et al., 1995). On a regional large scale, the  
460 relationship between mass balance and surge occurrence needs to be further ~~analysed~~analyzed. Our glacier elevation change  
461 maps of the period 2000-2010s are similar to that derived by Brun et al. (2017) and Shean et al. (2020). We found that, at the  
462 regional scale, the occurrence of surging glaciers is correlated with the regional glacier mass balance. The three subregions  
463 holding the largest clusters of surging glaciers, i.e., the Pamirs, Karakoram, and West Kunlun, are characterized by slightly  
464 negative or positive ~~mass budgets~~elevation changes, which is known as ~~the one part of the~~ ‘Pamir-Karakoram-West Kunlun’  
465 anomaly (Brun et al., 2017). Likewise, the subregions Central Tien Shan, Tibetan Interior Mountains, and East Kunlun Shan,  
466 which hold the moderate clusters of surging glaciers, have glacier mass loss rates much lower than the average rates of HMA.  
467 By contrast, subregions with severe glacier mass loss hold the lowest surging glacier ratio, such as the Dzhungarsky Alatau,  
468 Hengduan Shan, and Eastern Himalaya.

### 469 6.3 Comparison with previous surging glacier inventories

470 Guillet et al. (2022) presented a comprehensive surging glacier inventory of HMA for the period 2000-2018 from a multi-  
471 factor remote sensing approach. Prior to the comparison, we generated an inventory based on the RGI6.0, as Guillet et al.  
472 (2022) did. Guillet et al. (2022) identified 666 surging glaciers, and the area of surging glaciers occupies 19.5% of the total  
473 glacier area. We identified 890 surging glaciers (809 if ~~represented by RGI6.0 was used~~polygons), and their area only occupies  
474 16.59% of the total glacier area. We attributed the lower area ratio of surging glaciers to two reasons. First, in our inventory,  
475 the surging tributaries were separated from the non-surging trunks. Second, many outcrop rocks and shaded areas are excluded  
476 from the GAMDAM2 glacier areas (Sakai, 2019), which would lower our surging area ratio, but make the result more accurate.  
477 If we assign our identified surging glaciers to the RGI6.0 polygons without tributary separation, the surging area ratio would  
478 be larger (20.25%).

479 Within our inventory, 556 surging and 62 surge-like glaciers were also identified by Guillet et al. (2022), and the discrepancy  
480 of identifications mostly occurred on small glaciers. If only the period 2000-2020 was considered, 657 surging glaciers were  
481 identified by us, which is very close to that of Guillet et al. (665). For the period 1970s-2000, ~~there are~~151 surging and 101  
482 surge-like glaciers that were not identified by Guillet et al. (2022). Overall, we have newly identified 253 surging and 248  
483 surge-like glaciers. We owed the ~~newly new~~ findings to the longer observation period and multiple elevation change  
484 observations. However, 47 surging glaciers presented by Guillet et al. were missed in this study, and 62 surge-like glaciers in  
485 our new inventory were identified as surging glaciers by Guillet et al. (2022). We carefully checked the glaciers not included  
486 in our inventory but included in Guillet ~~et al et al.~~’s inventory, as well as those included in our inventory but not included in  
487 Guillet ~~et al et al.~~’s inventory, and this step helped us to find 21 more surging glaciers. We attribute this to the deficiency of  
488 using a single criterion, which could be aided by combining other features. Besides, the DEMs used in this study were suffering  
489 from ~~the~~ data voids and incomplete spatial coverage, especially for the KH-9 DEM, which could result in a relatively  
490 conservative identification.

491 Multiple studies have identified surging glaciers in the Karakoram based on different data sources. For example, Bhambri et  
492 al. (2017) identified 221 surging and surge-like glaciers (~~counting the~~ tributaries of a glacier system ~~are counted~~ as individual



493 glaciers) based on ~~the~~ glacier morphological changes detected from ~~spaceborne-space-borne~~ optical images acquired from  
494 1972 to 2016, in-situ observations, and archive photos ~~dating back to since~~ the 1840s. However, the boundary used by Bhambri  
495 et al. (2017) to define the extent of Karakoram is much smaller than that used in our inventory. A much smaller group of  
496 surging glaciers (88) ~~were~~ identified by Copland et al. (2011) based on a similar method and the data acquired between  
497 1960 and 2013. Rankl et al. (2014) identified 101 surging glaciers in the Karakoram by detecting ~~the~~ changes in glacier surface  
498 velocity and terminus position between 1976 and 2012. The results of Guillet et al. (2022) should be more reliable than previous  
499 ones, because more criteria were used for identifying surging glaciers. Compared with previous inventories, our inventory  
500 includes more surging glaciers (354). Among the 223 surging glaciers in the Karakoram identified by Guillet et al. (2022), 203  
501 were identified as surging glaciers, and 12 were identified as surge-like glaciers in this study, which means only 8 surging  
502 glaciers presented by Guillet et al. (2022) were not included in our inventory. The high coincidence between the two inventories  
503 indicates our surging glacier identification result is reliable. In total, we have newly identified 101 surging and 101 surge-like  
504 glaciers in this region.

505 Based on the method of glacier terminus change monitoring in Google Earth Engine, Vale et al. (2021) identified obvious  
506 terminus change of 137 surging glaciers. We found ~~that~~ 127 verified surging and 6 surge-like glaciers in our inventory were  
507 included in their inventory, i.e., only four glaciers were missed in this study. The possible reason for this gap is that the  
508 technique used by Vale et al. cannot identify the internal glacier surges ~~than-that~~ did not ~~cause-result in a~~ terminus  
509 ~~advancingadvance~~. Also, the inadequate quality and spatial resolution of satellite images could limit the performance of  
510 detecting changes in glacier terminus position.

511 In the Pamirs, Sevestre and Been (2015) identified 820 surge-type glaciers based on publications and reports, but Goerlich et  
512 al. (2020) reported only 186 surging glaciers based on ~~the~~ observations of glacier flow velocity, elevation change, etc. We  
513 found ~~that~~, if Goerlich et al. (2020) applied the GAMDAM2 glacier polygons used in this study, the number of identified  
514 surging glaciers ~~would should~~ be 182. Among the 182 surging glaciers identified by Goerlich et al. (2020), 153 ~~and 15~~ were  
515 identified as surging glaciers and ~~15 were identified as~~ surge-like glaciers in our study, ~~respectively~~. Although 14 surging  
516 glaciers are missed in this study, our inventory has contained other 94 surging and 44 surge-like glaciers. The main cause for  
517 the ~~result~~-discrepancy is that the glacier elevation change observation ~~before 2000~~ conducted by Goerlich et al. (2020) only  
518 covered ~~a small parts~~ of the Western Pamir ~~and only the observations before 2000 were used~~. In this region, our inventory  
519 shared 193 surging glaciers with Guillet ~~et al et al.~~'s inventory, and 185 of them were identified during the period 2000-2020,  
520 which also manifests a high coincidence of the two results.

521 In the West Kunlun, Yasuda and Furuya (2015) reported 9 surging glaciers in the main range only, based on changes in glacier  
522 flow velocity and terminus position of 31 glaciers, and ~~an~~ other 9 surging glaciers were found in the northwest part of the West  
523 Kunlun Shan by Chudley et al. (2019). A larger number (60) were found by Guillet et al. (2022). However, our inventory has  
524 even included more surging (82) and surge-like (47) glaciers in the West Kunlun Shan. During the period 2000-2020, we have  
525 identified 61 surging glaciers, which is very close to the number presented by Guillet et al. (2022). In Central Tien Shan,  
526 Mukherjee et al. (2017) identified 39 surge-type (including 9 surging and 13 very probable surging) glaciers through the  
527 analysis of changes in surface elevation and morphology from 1964 to 2014, whereas 79 (59 surging and 20 surge-like) were  
528 identified in our studies. The insufficient coverage of elevation change observation (only ~~covered-covering~~ the west part of the  
529 Central Tien Shan) may be the main reason for the discrepancy in identification results. Guillet et al. (2022) identified 54  
530 surging glaciers during 2000-2018, in which 36 were confirmed in our inventory.

## 531 7 Conclusions

532 This study present~~ed~~ a new inventory of surging glaciers across the entire HMA range, which was accomplished based on the  
533 glacier surface elevation changes derived from multiple elevation sources, by using the morphological changes from optical

534 images as complements. In total, 890 surging and 336 ~~surge-like~~probably or possibly surging glaciers were identified in the  
535 new inventory. Through the analysis of geometric parameters, we found that surging glaciers generally have a greater area,  
536 length, and elevation range than non-surging glaciers. However, the differences are smaller ~~when~~if taking the glacier size  
537 distribution into account. When considering glaciers of similar areas, the steeper ones are more likely to surge. Furthermore,  
538 ~~by~~ combining the region-wide glacier mass balance measurements, we found a similar distribution between the positive mass  
539 balance and ~~the~~ number of surging glaciers. Benefiting from the long period and wide coverage of surface elevation change  
540 observations, our study newly identified 253 surging and 248 surge-like glaciers in HMA than ~~the~~ previous inventory (Guillet  
541 et al., 2022). However, our inventory does not provide the surge duration period and the maximum flow velocity to describe  
542 the dynamic process of each glacier surge activity. Improvements should be made by combining multi-criteria identification  
543 methods. Considering the fact that glacier surges are more widespread than we thought, the inventory presented in this study  
544 still needs further replenishment.

## 545 **8 Data and code availability**

546 The presented inventory and corresponding multi-temporal elevation change results of identified surging glaciers are freely  
547 available at: <https://doi.org/10.5281/zenodo.7590838> (Guo et al., 2022). The inventory is distributed in the format of  
548 GeoPackage (.gpkg) and ESRI ~~shpfile~~shapefile (.shp), which is represented by outlines ~~or~~and manually defined center points  
549 of surging glaciers with geometric attributes. The glacier polygons of the inventory are compiled from the GAMDAM2 glacier  
550 inventory. In total, eight fields are integrated ~~into~~ the attributes table to describe the surging information of ~~the~~ corresponding  
551 glacier as mentioned in section 4.3. The description of each field in the attribute table is listed in Table 34. The DEM  
552 differencing results of ~~the~~ COP30 DEM ~~—~~ NASADEM, HMA~~8m~~ DEM ~~—~~ NASADEM, and NASADEM ~~—~~ KH-9 DEM are  
553 compressed into individual zip files, respectively. The elevation change results of surging glaciers were divided into multi-  
554 temporal  $1^\circ \times 1^\circ$  tiled GeoTiff grids. The metadata file is stored in a text file (README.txt), which contains the datasets  
555 description and details of the attribute information of the inventory.  
556 The code used for elevation change estimation can be available at: [https://github.com/TristanBlus/dem\\_coreg](https://github.com/TristanBlus/dem_coreg). This code was  
557 developed based on the *demcoreg* package (Shean et al., 2019).

## 558 **Author contribution**

559 J.L. and L.G. conceived this study and wrote the paper. L.G. developed the processing flow, compiled the inventory, and drew  
560 the figures with ~~the~~ support from J.L. A.D. generated the KH-9 DEM. A.D., Z.L., and X.L. helped with the results analysis  
561 and discussions, ~~and~~as well as manuscript editing. Z.L., J.L., and J.Z. provided ~~the~~ funding acquisition. All authors have  
562 contributed and agreed to the published version of the manuscript.

## 563 **Competing interest**

564 The authors declare that they have no conflict of interest.

## 565 **Acknowledgments**

566 The authors express ~~their~~ gratitude to all institutions that provide us ~~with~~ the opensource dataset used in this study: the NASA  
567 DEM from LP DAAC ([https://e4ftl01.cr.usgs.gov/MEASURES/NASADEM\\_HGT.001/](https://e4ftl01.cr.usgs.gov/MEASURES/NASADEM_HGT.001/)), the Copernicus DEM from  
568 ~~European~~European Space Agency (ESA) (<https://spacedata.copernicus.eu/web/cscda/cop-dem-faq>), the HMA~~8m~~ DEM  
569 processed by David Shean from National Snow and Ice Data Center (NSIDC)

570 ([https://insidc.org/data/HMA\\_DEM8m\\_MOS/versions/1](https://insidc.org/data/HMA_DEM8m_MOS/versions/1)), and the Randolph Glacier Inventory Version 6.0  
571 (<http://www.glims.org/RGI/andolph.html>). The authors also appreciate the valuable comments from Frank ~~Paul~~ Paul and  
572 Guillet Gregoire.

### 573 **Financial support**

574 This work was supported by the Strategic Priority Research Program of Chinese Academy of Sciences (XDA20100101), the  
575 National Natural Science Fund for Distinguished Young Scholars (41925016), the Hunan Key Laboratory of Remote Sensing  
576 of Ecological Environment in Dongting Lake Area (No. 2021-010), the National Natural Science Foundation of China  
577 (41904006), the Fundamental Research Funds for the Central Universities of Central South University (2021zzts0265).

### 578 **References**

- 579 Abdel Jaber, W., Rott, H., Floricioiu, D., Wuite, J., and Miranda, N.: Heterogeneous spatial and temporal pattern of surface  
580 elevation change and mass balance of the Patagonian ice fields between 2000 and 2016, *The Cryosphere*, 13, 2511–2535,  
581 doi:10.5194/tc-13-2511-2019, 2019.
- 582 AIRBUS: Copernicus Digital Elevation Model Validation Report, AIRBUS Defence and Space GmbH, 2020.
- 583 An, B., Wang, W., Yang, W., Wu, G., Guo, Y., Zhu, H., Gao, Y., Bai, L., Zhang, F., Zeng, C., Wang, L., Zhou, J., Li, X., Li,  
584 J., Zhao, Z., Chen, Y., Liu, J., Li, J., Wang, Z., Chen, W., and Yao, T.: Process, mechanisms, and early warning of glacier  
585 collapse-induced river blocking disasters in the Yarlung Tsangpo Grand Canyon, southeastern Tibetan Plateau, *Sci. Total*  
586 *Environ.*, 151652, doi:10.1016/j.scitotenv.2021.151652, 2021.
- 587 Barrand, N. E. and Murray, T.: Multivariate Controls on the Incidence of Glacier Surging in the Karakoram Himalaya, *Arct.*  
588 *Antarct. Alp. Res.*, 38, 489–498, doi:10.1657/1523-0430(2006)38[489:MCOTIO]2.0.CO;2, 2006.
- 589 Beaud, F., Aati, S., Delaney, I., Adhikari, S., and Avouac, J.-P.: Generalized sliding law applied to the surge dynamics of  
590 Shisper Glacier and constrained by timeseries correlation of optical satellite images, *Glaciers/Remote Sensing*, doi:10.5194/tc-  
591 2021-96, 2021.
- 592 Benn, D. I., Fowler, A. C., Hewitt, I., and Sevestre, H.: A general theory of glacier surges, *J. Glaciol.*, 65, 701–716,  
593 doi:10.1017/jog.2019.62, 2019.
- 594 Bhambri, R., Hewitt, K., Kawishwar, P., and Pratap, B.: Surge-type and surge-modified glaciers in the Karakoram, *Sci. Rep.*,  
595 7, doi:10.1038/s41598-017-15473-8, 2017.
- 596 Bhambri, R., Hewitt, K., Haritashya, U. K., Chand, P., Kumar, A., Verma, A., Tiwari, S. K., and Rai, S. K.: Characteristics of  
597 surge-type tributary glaciers, Karakoram, *Geomorphology*, 403, 108161, doi:10.1016/j.geomorph.2022.108161, 2022.
- 598 Bolch, T., Kulkarni, A., Kaab, A., Huggel, C., Paul, F., Cogley, J. G., Frey, H., Kargel, J. S., Fujita, K., Scheel, M., Bajracharya,  
599 S., and Stoffel, M.: The State and Fate of Himalayan Glaciers, *Science*, 336, 310–314, doi:10.1126/science.1215828, 2012.
- 600 Bolch, T., Pieczonka, T., Mukherjee, K., and Shea, J.: Brief communication: Glaciers in the Hunza catchment (Karakoram)  
601 have been nearly in balance since the 1970s, *The Cryosphere*, 11, 531–539, doi:10.5194/tc-11-531-2017, 2017.
- 602 Bolch, T., Shea, J. M., Liu, S., Azam, F. M., Gao, Y., Gruber, S., Immerzeel, W. W., Kulkarni, A., Li, H., Tahir, A. A., Zhang,  
603 G., and Zhang, Y.: Status and Change of the Cryosphere in the Extended Hindu Kush Himalaya Region, in: *The Hindu Kush*  
604 *Himalaya Assessment*, edited by: Wester, P., Mishra, A., Mukherji, A., and Shrestha, A. B., Springer International Publishing,  
605 Cham, 209–255, doi:10.1007/978-3-319-92288-1\_7, 2019.
- 606 Brun, F., Berthier, E., Wagnon, P., Käab, A., and Treichler, D.: A spatially resolved estimate of High Mountain Asia glacier  
607 mass balances from 2000 to 2016, *Nat. Geosci.*, 10, 668–673, doi:10.1038/ngeo2999, 2017.
- 608 Chudley, T. R. and Willis, I. C.: Glacier surges in the north-west West Kunlun Shan inferred from 1972 to 2017 Landsat  
609 imagery, *J. Glaciol.*, 65, 1–12, doi:10.1017/jog.2018.94, 2019.

610 Clarke, G. K. C.: Length, width and slope influences on glacier surging, *J. Glaciol.*, 37, 236–246,  
611 doi:10.3189/S0022143000007255, 1991.

612 Clarke, G. K. C., Schmok, J. P., Ommanney, C. S. L., and Collins, S. G.: Characteristics of surge-type glaciers, *J. Geophys.*  
613 *Res. Solid Earth*, 91, 7165–7180, doi:10.1029/JB091iB07p07165, 1986.

614 Cogley, J. G., Arendt, A. A., Bauder, A., Braithwaite, R. J., Hock, R., J, B., R., Jansson, P., Kaser, G., Moller, M., Nicholson,  
615 L., Rasmussen, L. A., and Zemp, M.: Glossary of glacier mass balance and related terms, IACS Contribution No.2, UNESCO,  
616 Paris, 2011.

617 Copland, L., Sylvestre, T., Bishop, M. P., Shroder, J. F., Seong, Y. B., Owen, L. A., Bush, A., and Kamp, U.: Expanded and  
618 Recently Increased Glacier Surging in the Karakoram, *Arct. Antarct. Alp. Res.*, 43, 503–516, 2011.

619 Crippen, R., Buckley, S., Agram, P., Belz, E., Gurrola, E., Hensley, S., Kobrick, M., Lavallo, M., Martin, J., Neumann, M.,  
620 Nguyen, Q., Rosen, P., Shimada, J., Simard, M., and Tung, W.: NASADEM global elevation model: methods and progress,  
621 *ISPRS - Int. Arch. Photogramm. Remote Sens. Spat. Inf. Sci.*, XLI-B4, 125–128, doi:10.5194/isprsarchives-XLI-B4-125-2016,  
622 2016.

623 Dehecq, A., Gardner, A. S., Alexandrov, O., McMichael, S., Hugonnet, R., Shean, D., and Marty, M.: Automated Processing  
624 of Declassified KH-9 Hexagon Satellite Images for Global Elevation Change Analysis Since the 1970s, *Front. Earth Sci.*, 8,  
625 566802, doi:10.3389/feart.2020.566802, 2020.

626 Dowdeswell, J. A., Hodgkins, R., Nuttall, A.-M., Hagen, J. O., and Hamilton, G. S.: Mass balance change as a control on the  
627 frequency and occurrence of glacier surges in Svalbard, Norwegian High Arctic, *Geophys. Res. Lett.*, 22, 2909–2912,  
628 doi:10.1029/95GL02821, 1995.

629 Eisen, O., Harrison, W. D., Raymond, C. F., Echelmeyer, K. A., Bender, G. A., and Gorda, J. L. D.: Variegated Glacier, Alaska,  
630 USA: a century of surges, *J. Glaciol.*, 51, 399–406, doi:10.3189/172756505781829250, 2005.

631 Fan, Y., Ke, C.-Q., Zhou, X., Shen, X., Yu, X., and Lhakpa, D.: Glacier mass-balance estimates over High Mountain Asia  
632 from 2000 to 2021 based on ICESat-2 and NASADEM, *J. Glaciol.*, 1–13, doi:10.1017/jog.2022.78, 2022.

633 Farinotti, D., Immerzeel, W. W., Kok, R., Quincey, D. J., and Dehecq, A.: Manifestations and mechanisms of the Karakoram  
634 glacier Anomaly, *Nat. Geosci.*, 13, 8–16, doi:10.1038/s41561-019-0513-5, 2020.

635 Farnsworth, W. R., Ingólfsson, Ó., Retelle, M., and Schomacker, A.: Over 400 previously undocumented Svalbard surge-type  
636 glaciers identified, *Geomorphology*, 264, 52–60, doi:10.1016/j.geomorph.2016.03.025, 2016.

637 Farr, T. G., Rosen, P. A., Caro, E., Crippen, R., Duren, R., Hensley, S., Kobrick, M., Paller, M., Rodriguez, E., Roth, L., Seal,  
638 D., Shaffer, S., Shimada, J., Umland, J., Werner, M., Oskin, M., Burbank, D., and Alsdorf, D.: The Shuttle Radar Topography  
639 Mission, *Rev. Geophys.*, 45, RG2004, doi:10.1029/2005RG000183, 2007.

640 Fowler, A. C.: A theory of glacier surges, *J. Geophys. Res.*, 92, 9111, doi:10.1029/JB092iB09p09111, 1987.

641 Fowler, A. C., Murray, T., and Ng, F. S. L.: Thermally controlled glacier surging, *J. Glaciol.*, 47, 527–538,  
642 doi:10.3189/172756501781831792, 2001.

643 Gardelle, J., Berthier, E., Arnaud, Y., and Käab, A.: Region-wide glacier mass balances over the Pamir-Karakoram-Himalaya  
644 during 1999–2011, *Cryosphere Discuss.*, 7, 975–1028, doi:10.5194/tcd-7-975-2013, 2013.

645 Goerlich, F., Bolch, T., and Paul, F.: More dynamic than expected: an updated survey of surging glaciers in the Pamir, *Earth*  
646 *Syst. Sci. Data*, 12, 3161–3176, doi:10.5194/essd-12-3161-2020, 2020.

647 Guillet, G., King, O., Lv, M., Ghuffar, S., Benn, D., Quincey, D., and Bolch, T.: A regionally resolved inventory of High  
648 Mountain Asia surge-type glaciers, derived from a multi-factor remote sensing approach, *The Cryosphere*, 16, 603–623,  
649 doi:10.5194/tc-16-603-2022, 2022.

650 Guth, P. L. and Geoffroy, T. M.: LiDAR point cloud and ICESat-2 evaluation of 1 second global digital elevation models:  
651 Copernicus wins, *Trans. GIS*, 25, 2245–2261, doi:10.1111/tgis.12825, 2021.

652 Hewitt, K.: The Karakoram Anomaly? Glacier Expansion and the 'Elevation Effect,' *Karakoram Himalaya, Mt. Res. Dev.*, 25,  
653 332–340, doi:10.1659/0276-4741(2005)025[0332:TKAGEA]2.0.CO;2, 2005.

654 Hewitt, K.: Tributary glacier surges: an exceptional concentration at Panmah Glacier, Karakoram Himalaya, *J. Glaciol.*, 53,  
655 181–188, doi:10.3189/172756507782202829, 2007.

656 Höhle, J. and Höhle, M.: Accuracy assessment of digital elevation models by means of robust statistical methods, *ISPRS J.*  
657 *Photogramm. Remote Sens.*, 64, 398–406, doi:10.1016/j.isprsjprs.2009.02.003, 2009.

658 Holzer, N., Vijay, S., Yao, T., Xu, B., Buchroithner, M., and Bolch, T.: Four decades of glacier variations at Muztagh Ata  
659 (eastern Pamir): a multi-sensor study including Hexagon KH-9 and Pléiades data, *The Cryosphere*, 9, 2071–2088,  
660 doi:10.5194/tc-9-2071-2015, 2015.

661 Hugonnet, R., McNabb, R., Berthier, E., Menounos, B., Nuth, C., Girod, L., Farinotti, D., Huss, M., Dussailant, I., Brun, F.,  
662 and Kääb, A.: Accelerated global glacier mass loss in the early twenty-first century, *Nature*, 592, 726–731,  
663 doi:10.1038/s41586-021-03436-z, 2021.

664 Jacquemart, M. and Cicoira, A.: Hazardous Glacier Instabilities: Ice Avalanches, Sudden Large-Volume Detachments of Low-  
665 Angle Mountain Glaciers, and Glacier Surges, in: *Treatise on Geomorphology*, Elsevier, 330–345, doi:10.1016/B978-0-12-  
666 818234-5.00188-7, 2022.

667 Jiskoot, H.: Glacier Surging, in: *Encyclopedia of Snow, Ice and Glaciers*, edited by: Singh, V. P., Singh, P., and Haritashya,  
668 U. K., Springer Netherlands, Dordrecht, 415–428, doi:10.1007/978-90-481-2642-2\_559, 2011.

669 Jiskoot, H., Murray, T., and Boyle, P.: Controls on the distribution of surge-type glaciers in Svalbard, *J. Glaciol.*, 46, 412–422,  
670 doi:10.3189/172756500781833115, 2000.

671 Kääb, A., Leinss, S., Gilbert, A., Bühler, Y., Gascoïn, S., Evans, S. G., Bartelt, P., Berthier, E., Brun, F., Chao, W.-A., Farinotti,  
672 D., Gimbert, F., Guo, W., Huggel, C., Kargel, J. S., Leonard, G. J., Tian, L., Treichler, D., and Yao, T.: Massive collapse of  
673 two glaciers in western Tibet in 2016 after surge-like instability, *Nat. Geosci.*, 11, 114–120, doi:10.1038/s41561-017-0039-7,  
674 2018.

675 Kääb, A., Jacquemart, M., Gilbert, A., Leinss, S., Girod, L., Huggel, C., Falaschi, D., Ugalde, F., Petrakov, D., Chernomorets,  
676 S., Dokukin, M., Paul, F., Gascoïn, S., Berthier, E., and Kargel, J. S.: Sudden large-volume detachments of low-angle mountain  
677 glaciers – more frequent than thought?, *The Cryosphere*, 15, 1751–1785, doi:10.5194/tc-15-1751-2021, 2021.

678 Kamb, B.: Glacier surge mechanism based on linked cavity configuration of the basal water conduit system, *J. Geophys. Res.*,  
679 92, 9083, doi:10.1029/JB092iB09p09083, 1987.

680 Kochtitzky, W., Winski, D., McConnell, E., Kreutz, K., Campbell, S., Enderlin, E. M., Copland, L., Williamson, S., Main, B.,  
681 and Jiskoot, H.: Climate and surging of Donjek Glacier, Yukon, Canada, *Arct. Antarct. Alp. Res.*, 52, 264–280,  
682 doi:10.1080/15230430.2020.1744397, 2020.

683 Li, J., Li, Z., Zhu, J., Li, X., Xu, B., Wang, Q., Huang, C., and Hu, J.: Early 21st century glacier thickness changes in the  
684 Central Tien Shan, *Remote Sens. Environ.*, 192, 12–29, doi:10.1016/j.rse.2017.02.003, 2017.

685 Lv, M., Guo, H., Lu, X., Liu, G., Yan, S., Ruan, Z., Ding, Y., and Quincey, D. J.: Characterizing the behaviour of surge- and  
686 non-surge-type glaciers in the Kingata Mountains, eastern Pamir, from 1999 to 2016, *The Cryosphere*, 13, 219–236,  
687 doi:10.5194/tc-13-219-2019, 2019.

688 Lv, M., Guo, H., Yan, J., Wu, K., Liu, G., Lu, X., Ruan, Z., and Yan, S.: Distinguishing Glaciers between Surging and  
689 Advancing by Remote Sensing: A Case Study in the Eastern Karakoram, *Remote Sens.*, 12, 2297, doi:10.3390/rs12142297,  
690 2020.

691 Maurer, J. M., Schaefer, J. M., Rupper, S., and Corley, A.: Acceleration of ice loss across the Himalayas over the past 40 years,  
692 *Sci. Adv.*, 5, eaav7266, doi:10.1126/sciadv.aav7266, 2019.

693 Maussion, F., Scherer, D., Mölg, T., Collier, E., Curio, J., and Finkelnburg, R.: Precipitation Seasonality and Variability over  
694 the Tibetan Plateau as Resolved by the High Asia Reanalysis, *J. Clim.*, 27, 1910–1927, doi:10.1175/JCLI-D-13-00282.1, 2014.



695 Maussion, F., Butenko, A., Champollion, N., Dusch, M., Eis, J., Fourteau, K., Gregor, P., Jarosch, A. H., Landmann, J.,  
696 Oesterle, F., Recinos, B., Rothenpieler, T., Vlug, A., Wild, C. T., and Marzeion, B.: The Open Global Glacier Model (OGGM)  
697 v1.1, *Geosci. Model Dev.*, 12, 909–931, doi:10.5194/gmd-12-909-2019, 2019.

698 Muhammad, S., Li, J., Steiner, J. F., Shrestha, F., Shah, G. M., Berthier, E., Guo, L., Wu, L., and Tian, L.: A holistic view of  
699 Shisper Glacier surge and outburst floods: from physical processes to downstream impacts, *Geomat. Nat. Hazards Risk*, 12,  
700 2755–2775, doi:10.1080/19475705.2021.1975833, 2021.

701 Mukherjee, K., Bolch, T., Goerlich, F., Kutuzov, S., Osmonov, A., Pieczonka, T., and Shesterova, I.: Surge-Type Glaciers in  
702 the Tien Shan (Central Asia), *Arct. Antarct. Alp. Res.*, 49, 147–171, doi:10.1657/AAAR0016-021, 2017.

703 Murray, T., Strozzii, T., Luckman, A., Jiskoot, H., and Christakos, P.: Is there a single surge mechanism? Contrasts in dynamics  
704 between glacier surges in Svalbard and other regions: IS THERE A SINGLE SURGE MECHANISM?, *J. Geophys. Res. Solid*  
705 *Earth*, 108, doi:10.1029/2002JB001906, 2003.

706 Nuimura, T., Sakai, A., Taniguchi, K., Nagai, H., Lamsal, D., Tsutaki, S., Kozawa, A., Hoshina, Y., Takenaka, S., Omiya, S.,  
707 Tsunematsu, K., Tshering, P., and Fujita, K.: The GAMDAM glacier inventory: a quality-controlled inventory of Asian  
708 glaciers, *The Cryosphere*, 9, 849–864, doi:10.5194/tc-9-849-2015, 2015.

709 Nuth, C. and Kääb, A.: Co-registration and bias corrections of satellite elevation data sets for quantifying glacier thickness  
710 change, *The Cryosphere*, 5, 271–290, doi:10.5194/tc-5-271-2011, 2011.

711 Paul, F.: Revealing glacier flow and surge dynamics from animated satellite image sequences: examples from the Karakoram,  
712 *The Cryosphere*, 9, 2201–2214, doi:10.5194/tc-9-2201-2015, 2015.

713 Paul, F.: Repeat Glacier Collapses and Surges in the Amney Machen Mountain Range, Tibet, Possibly Triggered by a  
714 Developing Rock-Slope Instability, *Remote Sens.*, 11, 708, doi:10.3390/rs11060708, 2019.

715 Purinton, B. and Bookhagen, B.: Beyond Vertical Point Accuracy: Assessing Inter-pixel Consistency in 30 m Global DEMs  
716 for the Arid Central Andes, *Front. Earth Sci.*, 9, 758606, doi:10.3389/feart.2021.758606, 2021.

717 Quincey, D. J., Braun, M., Glasser, N. F., Bishop, M. P., Hewitt, K., and Luckman, A.: Karakoram glacier surge dynamics,  
718 *Geophys. Res. Lett.*, 38, L18504, doi:10.1029/2011GL049004, 2011.

719 Rankl, M., Kienholz, C., and Braun, M.: Glacier changes in the Karakoram region mapped by multitemission satellite imagery,  
720 *The Cryosphere*, 8, 977–989, doi:10.5194/tc-8-977-2014, 2014.

721 Round, V., Leinss, S., Huss, M., Haemmig, C., and Hajnsek, I.: Surge dynamics and lake outbursts of Kyagar Glacier,  
722 Karakoram, *The Cryosphere*, 11, 723–739, doi:10.5194/tc-11-723-2017, 2017.

723 Sakai, A.: Brief communication: Updated GAMDAM glacier inventory over high-mountain Asia, *The Cryosphere*, 13, 2043–  
724 2049, doi:10.5194/tc-13-2043-2019, 2019.

725 Sevestre, H. and Benn, D. I.: Climatic and geometric controls on the global distribution of surge-type glaciers: implications  
726 for a unifying model of surging, *J. Glaciol.*, 61, 646–662, doi:10.3189/2015JoG14J136, 2015.

727 Shean, D., Shashank Bhushan, Lilien, D., and Meyer, J.: dshean/demcoreg: Zenodo DOI release, —, —,  
728 doi:10.5281/ZENODO.3243481, 2019.

729 Shean, D. E., Alexandrov, O., Moratto, Z. M., Smith, B. E., Joughin, I. R., Porter, C., and Morin, P.: An automated, open-  
730 source pipeline for mass production of digital elevation models (DEMs) from very-high-resolution commercial stereo satellite  
731 imagery, *ISPRS J. Photogramm. Remote Sens.*, 116, 101–117, doi:10.1016/j.isprsjprs.2016.03.012, 2016.

732 Shean, D. E., Bhushan, S., Montesano, P., Rounce, D. R., Arendt, A., and Osmanoglu, B.: A Systematic, Regional Assessment  
733 of High Mountain Asia Glacier Mass Balance, *Front. Earth Sci.*, 7, 363, doi:10.3389/feart.2019.00363, 2020.

734 Steiner, J. F., Kraaijenbrink, P. D. A., Jiduc, S. G., and Immerzeel, W. W.: Brief communication: The Khurdopin glacier surge  
735 revisited – extreme flow velocities and formation of a dammed lake in 2017, *The Cryosphere*, 12, 95–101, doi:10.5194/tc-12-  
736 95-2018, 2018.

- 737 Surazakov, A. and Aizen, V.: Positional Accuracy Evaluation of Declassified Hexagon KH-9 Mapping Camera Imagery,  
 738 Photogramm. Eng. Remote Sens., 76, 603–608, doi:10.14358/PERS.76.5.603, 2010.
- 739 Thøgersen, K., Gilbert, A., Schuler, T. V., and Malthé-Sørenssen, A.: Rate-and-state friction explains glacier surge propagation,  
 740 Nat. Commun., 10, 2823, doi:10.1038/s41467-019-10506-4, 2019.
- 741 Vale, A. B., Arnold, N. S., Rees, W. G., and Lea, J. M.: Remote Detection of Surge-Related Glacier Terminus Change across  
 742 High Mountain Asia, Remote Sens., 13, 1309, doi:10.3390/rs13071309, 2021.
- 743 Van Wyk de Vries, M., Wickert, A. D., MacGregor, K. R., Rada, C., and Willis, M. J.: Atypical landslide induces speedup,  
 744 advance, and long-term slowdown of a tidewater glacier, Geology, doi:10.1130/G49854.1, 2022.
- 745 Yamazaki, D., Ikeshima, D., Tawatari, R., Yamaguchi, T., O’Loughlin, F., Neal, J. C., Sampson, C. C., Kanae, S., and Bates,  
 746 P. D.: A high-accuracy map of global terrain elevations, Geophys. Res. Lett., 44, 5844–5853, doi:10.1002/2017GL072874,  
 747 2017.
- 748 Yasuda, T. and Furuya, M.: Dynamics of surge-type glaciers in West Kunlun Shan, Northwestern Tibet, J. Geophys. Res.  
 749 Earth Surf., 120, 2393–2405, doi:10.1002/2015JF003511, 2015.
- 750 Zhou, S., Yao, X., Zhang, D., Zhang, Y., Liu, S., and Min, Y.: Remote Sensing Monitoring of Advancing and Surging Glaciers  
 751 in the Tien Shan, 1990–2019, Remote Sens., 13, 1973, doi:10.3390/rs13101973, 2021.
- 752 Zhou, Y., Li, Z., and Li, J.: Slight glacier mass loss in the Karakoram region during the 1970s to 2000 revealed by KH-9  
 753 images and SRTM DEM, J. Glaciol., 63, 331–342, doi:10.1017/jog.2016.142, 2017.
- 754 Zhou, Y., Li, Z., Li, J., Zhao, R., and Ding, X.: Glacier mass balance in the Qinghai–Tibet Plateau and its surroundings from  
 755 the mid-1970s to 2000 based on Hexagon KH-9 and SRTM DEMs, Remote Sens. Environ., 210, 96–112,  
 756 doi:10.1016/j.rse.2018.03.020, 2018.

## 757 Tables and Figures

758 **Table 1: Surging glacier identification results**

Glacier changes	Identification class			Total
	I	II	III	
2000-2020 elevation change	719	157	169	1045
1970s-2000 elevation change	507	156	57	720
1986-2021 terminus advance	247	397	-	645
1986-2021 looped moraine	112	31	-	144
1986-2021 medial moraine	69	29	-	108
<b>Final identified surging glaciers</b>	890 (verified)	208 (probable)	128 (possible)	1226

759

760 **Table 2: Results of surging glacier identification in 22 subregions of HMA. Only glaciers larger than 0.4 km<sup>2</sup> were considered**  
 761 **in the glacier number related values.**

HiMAP regions	Glacier Number				Glacier Area			
	Surging	Surge-like	Total	Ratio (%)	Surging	Surge-like	Total	Ratio (%)
Karakoram	354	128	4121	8.59	7936.12	1329.40	20103.68	39.48
Western Pamir	188	48	3058	6.15	2232.52	289.597	8172.64	27.32
Western Kunlun Shan	82	47	2508	3.27	2580.21	589.17	8466.12	30.48
Central Tien Shan	59	20	2248	2.62	881.61	305.47	6816.95	12.93
Eastern Pamir	56	16	1148	4.88	796.35	79.12	2746.47	29.00
Tanggula Shan	22	4	697	3.16	441.94	41.71	1937.39	22.81
Tibetan Interior Mountains	22	12	1471	1.50	286.29	140.22	3933.48	7.28
Northern Western Tien Shan	21	6	1374	1.53	116.27	81.09	2502.60	4.65

Central Himalaya	17	21	3433	0.50	164.12	185.07	9928.72	1.65
Eastern Kunlun Shan	16	7	1191	1.34	458.11	55.38	2960.26	15.48
Nyainqentanglha	10	5	2916	0.34	119.53	184.79	7216.62	1.66
Eastern Hindu Kush	9	5	1279	0.70	178.18	77.19	3055.80	5.83
Western Himalaya	9	4	3659	0.25	110.22	69.41	8619.19	1.28
Eastern Himalaya	6	0	1334	0.45	94	0	3371.89	2.79
Pamir Alay	5	0	991	0.50	35.72	0	1957.94	1.82
Qilian Shan	4	6	851	0.47	35.99	26.40	1627.94	2.21
Eastern Tibetan Mountains	3	2	156	1.92	36.33	3.85	341.46	10.64
Altun Shan	2	3	156	1.28	4.13	3.17	294.95	1.40
Eastern Tien Shan	2	1	1243	0.16	12.03	2.59	2440.11	0.49
Hengduan Shan	2	0	700	0.29	26.22	0	1335.39	1.96
Gangdise Mountains	1	0	768	0.13	10.52	0	1339.54	0.79
Dzhungarsky Alatau	0	1	407	0	0	10.98	648.61	0
<b>Total</b>	<b>890</b>	<b>336</b>	<b>35709</b>	<b>2.49</b>	<b>16556.42</b>	<b>3474.60</b>	<b>99817.72</b>	<b>16.59</b>

762 \* The value of ratio only considered the number and area of surging glaciers.

763

764 **Table 3: The number and area ratios of surging glaciers in all glaciers for different area classes.**

Area Class	Total		Surging Glacier		Ratio (%)	
	Count	Area (km <sup>2</sup> )	Count	Area (km <sup>2</sup> )	Count	Area
0.4-1	19428	12215.4	28	20.8	0.14	0.17
1-3	10983	18305.7	169	345.0	1.54	1.88
3-5	2404	9229.4	141	560.3	5.87	6.07
5-10	1650	11370.1	195	1416.4	11.82	12.46
10-30	946	15048.9	227	3861.2	24.00	25.66
30-50	161	5979.1	56	2036.5	34.78	34.06
50-100	92	6337.4	48	3329.2	52.17	52.53
100-300	39	6191.4	24	3651.5	61.54	58.98
≥300	6	3466.3	2	1335.6	33.33	38.53

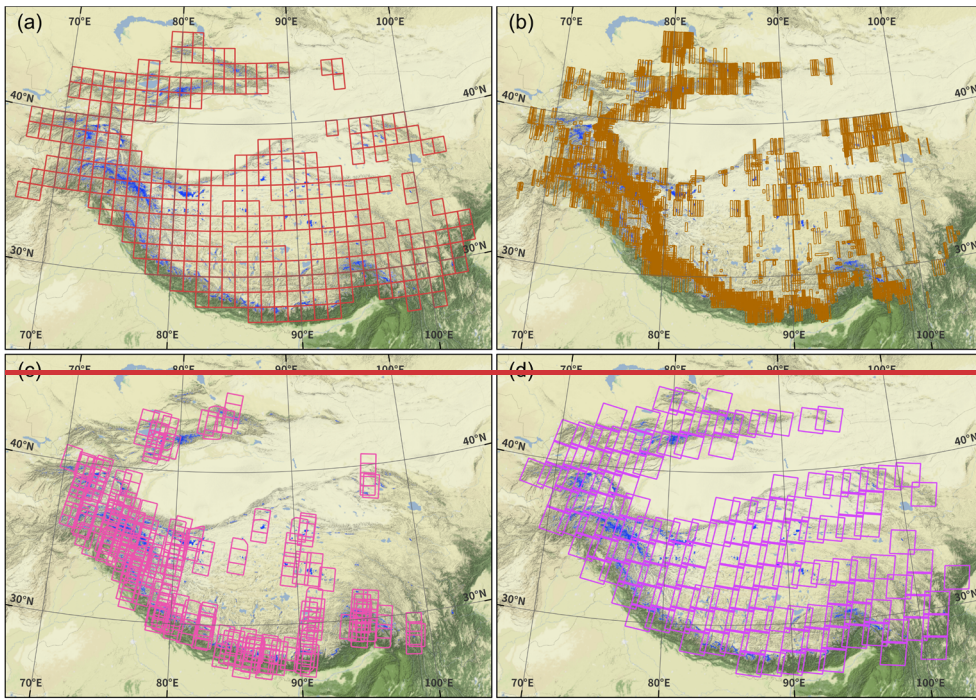
765

766 **Table 34: Attribute information in the present surging glacier inventory.**

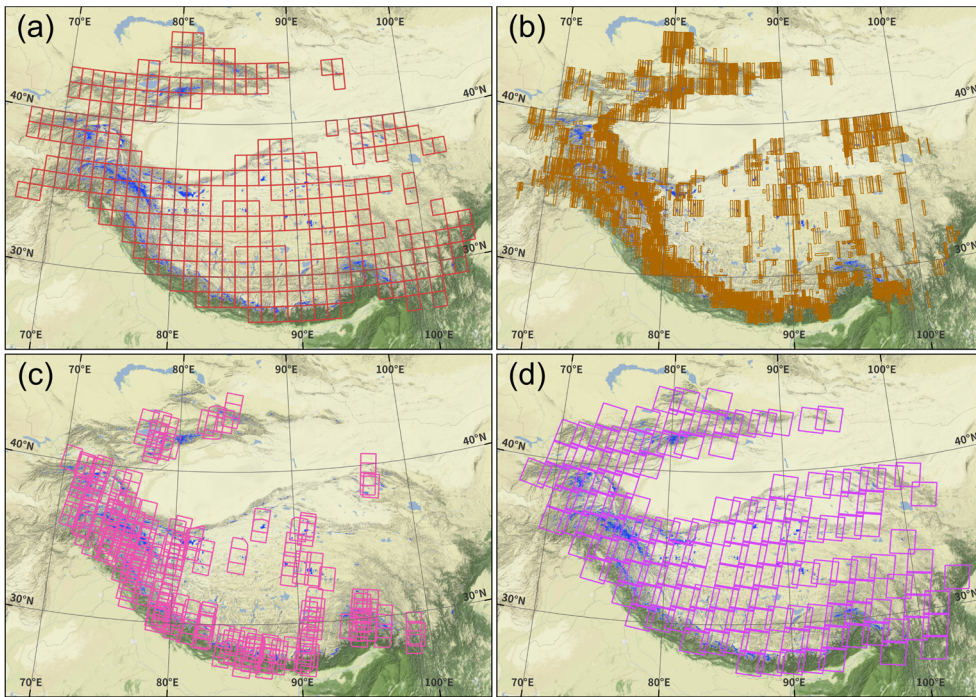
Attribute	Description	Attribute	Description
Glac_ID	Glacier identifier composed by Lat/Lon	Surge_20	Surge identified in 2000-2020 by dH
Area	Glacier area (km <sup>2</sup> )	Surge_70s	Surge identified in 1970s-2000 by dH
Zmin	Minimum elevation of the glacier (m a.s.l)	Delta_T	Identified class of glacier terminus advance
Zmax	Maximum elevation of the glacier (m a.s.l)	Loop_M	Identified class of looped moraine change
Zmed	Median elevation of the glacier (m a.s.l)	Medial_M	Identified class of medial moraine change
Slope	Mean glacier surface slope (°)	False_signal	False positive signal of identification
Aspect	Mean glacier aspect/orientation (°)	Trib_surge	If the glacier has/is surging tributary
MaxL	Maximum length of glacier flow line (m)	Surge_class	Final surge identification during 1970s-2020
HiMAP_region	HMA subregion that the glacier belongs to		

767



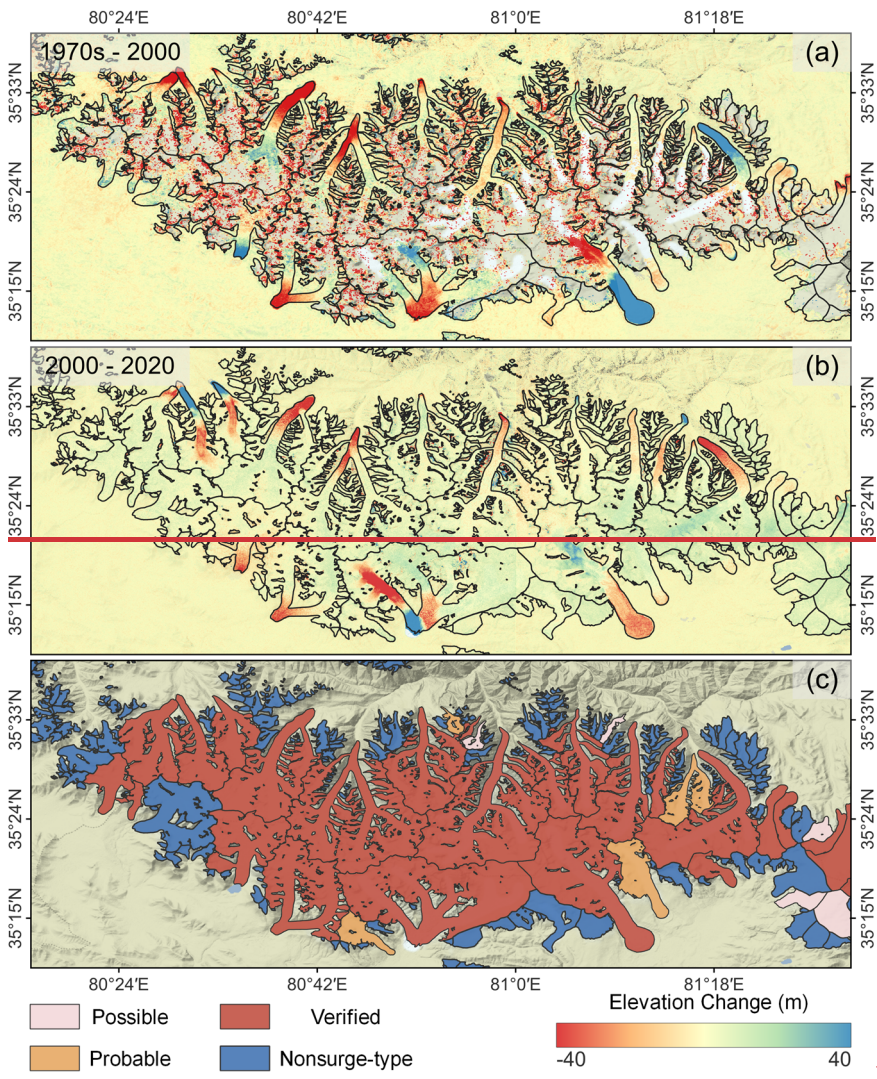


□ COP30 DEM/NASADEM Footprint (313 tiles)      □ HMA8m DEM Footprint (3598 tiles)  
□ KH-9 DEM Footprint (238 tiles)                      □ Landsat images Footprint (148 frames)

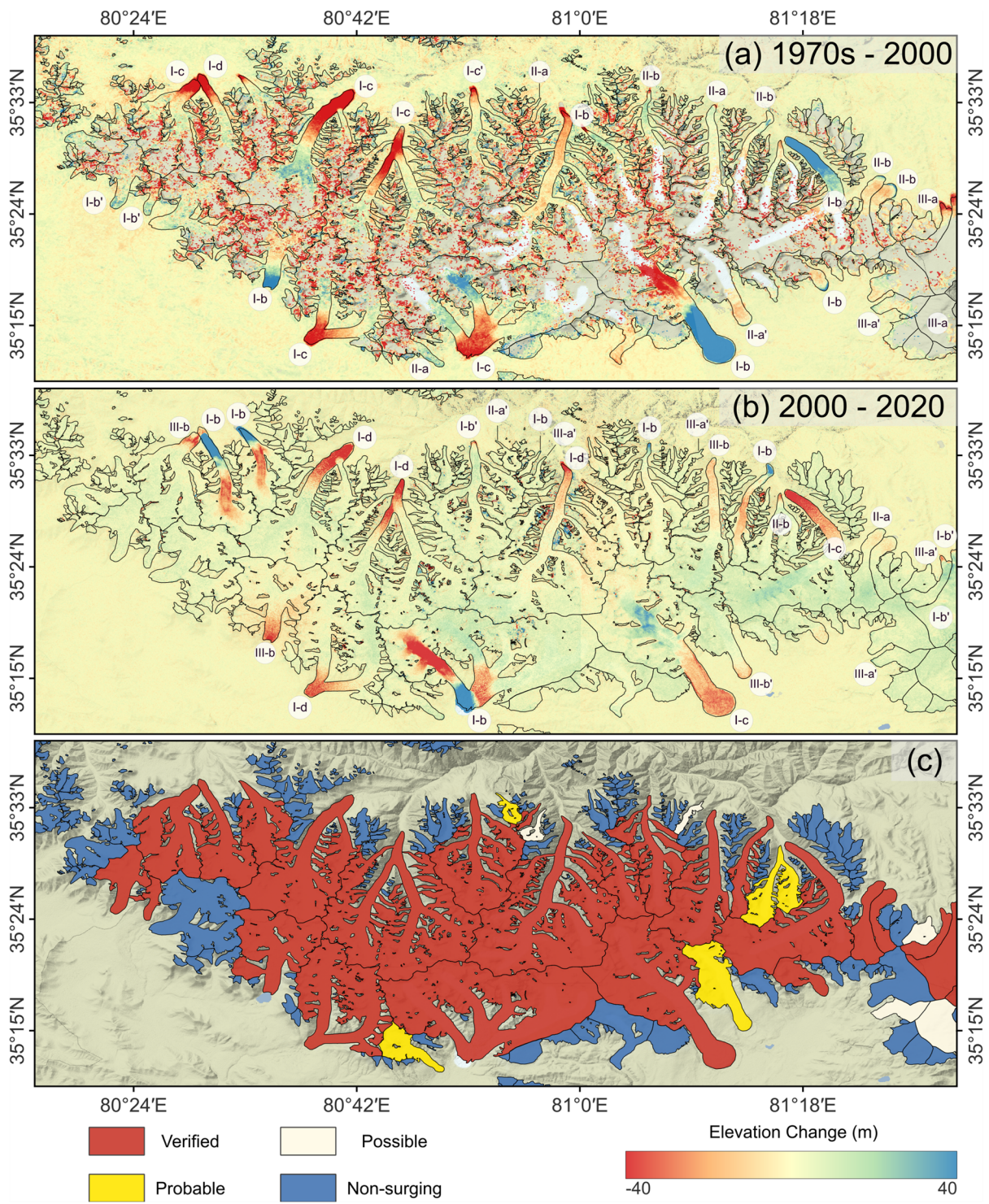


□ COP30 DEM/NASADEM Footprint (313 tiles)      □ HMA DEM Footprint (3598 tiles)  
□ KH-9 DEM Footprint (238 tiles)                      □ Landsat images Footprint (148 frames)

Figure 1: Footprints of (a) the COP30/NASA DEMs, (b) the HMA8m DEMs, (c) the KH-9 DEMs, and (d) Landsat imageries that were utilized in this study. The background is rendered from the ESRI World Physical base map (Source: US National Park Service).



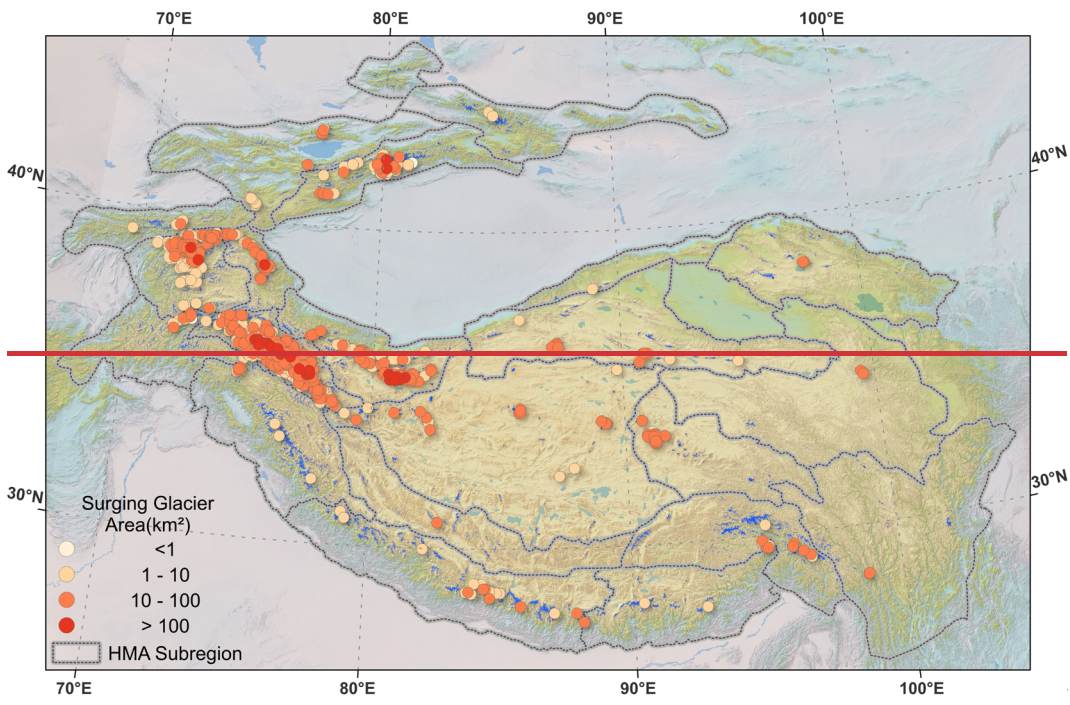




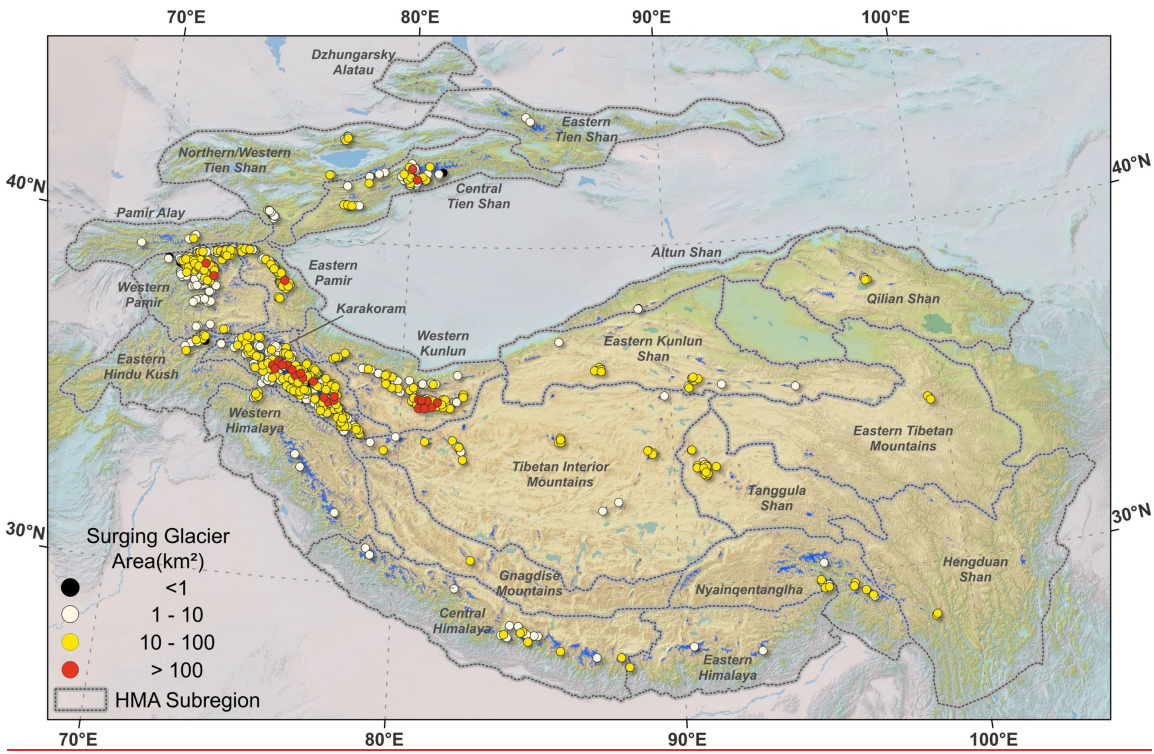
773

774 **Figure 2: An example of derived elevation change maps during (a) 1970s-2000 (a) and (b) 2000-2020 (b), and (c) the corresponding**  
 775 **surging glacier identification results (c). Black curves are glacier outlines. The labels in panels (a) and (b) represent the identified**  
 776 **classes based on the elevation change patterns (the criteria of identification is elaborated in section 4.2.1). The subscript ‘’ in the**  
 777 **labels indicates that the surging glacier is identified by combining other elevation change maps. The background is the shaded relief**  
 778 **of the COP30 DEM (Source: ESA). The area is in the main massif of Western Kunlun Shan.**





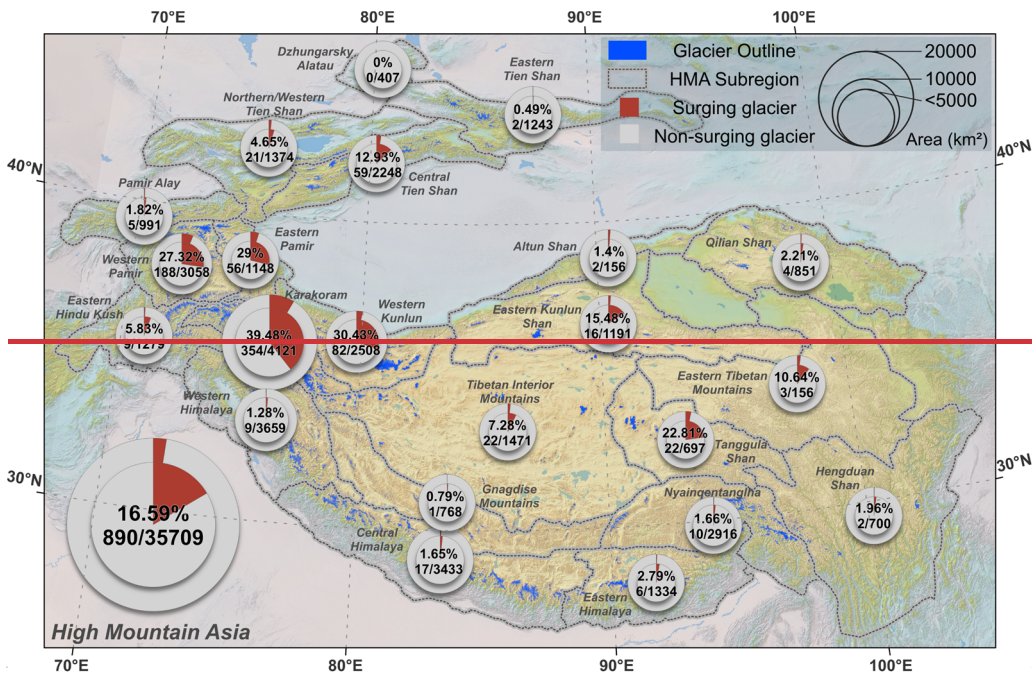
779



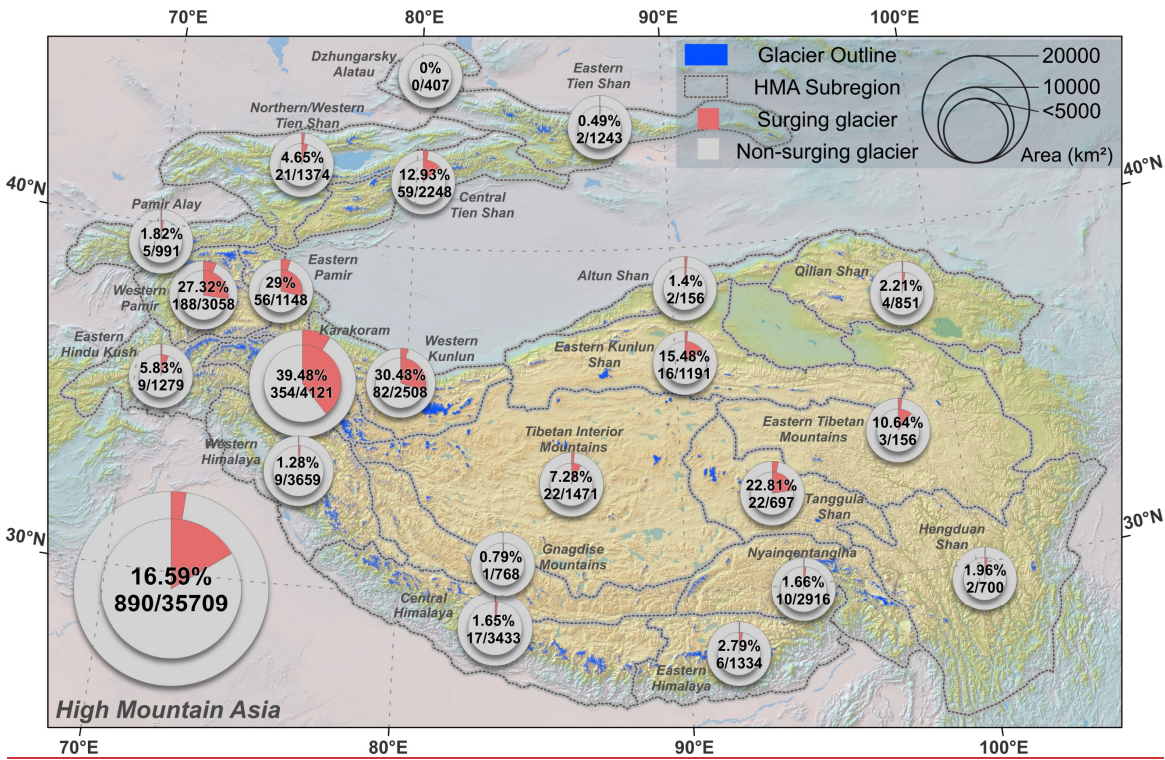
780

781 **Figure 3: Overview of the distribution of identified surging glaciers in 22 subregions of HMA. The background is the shaded relief**  
 782 **of SRTM DEM (Source: USGS).**





783

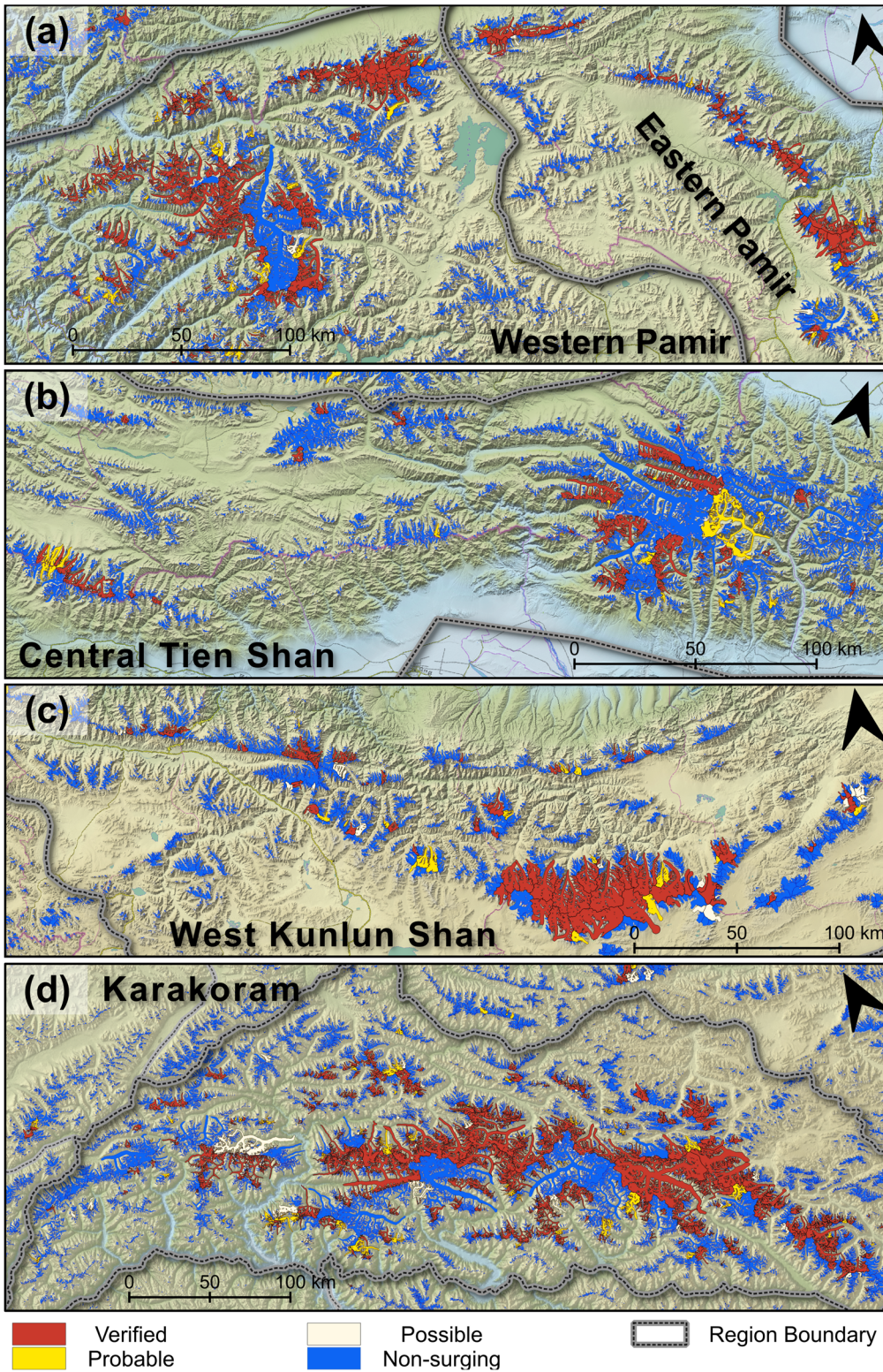


784

785 **Figure 4: Distribution of surging glaciers in the 22 subregions of HMA. The double-level pie chart represents the ratios of surging**  
 786 **glacier number and area in each subregion. The inner pie denotes the area ratio labeled by a percentage, and the outer pie denotes**  
 787 **the number ratio labeled by a fraction (only considered glaciers larger than 0.4 km<sup>2</sup> are considered).** The background is the shaded  
 788 **relief of SRTM DEM (Source: USGS).**







791

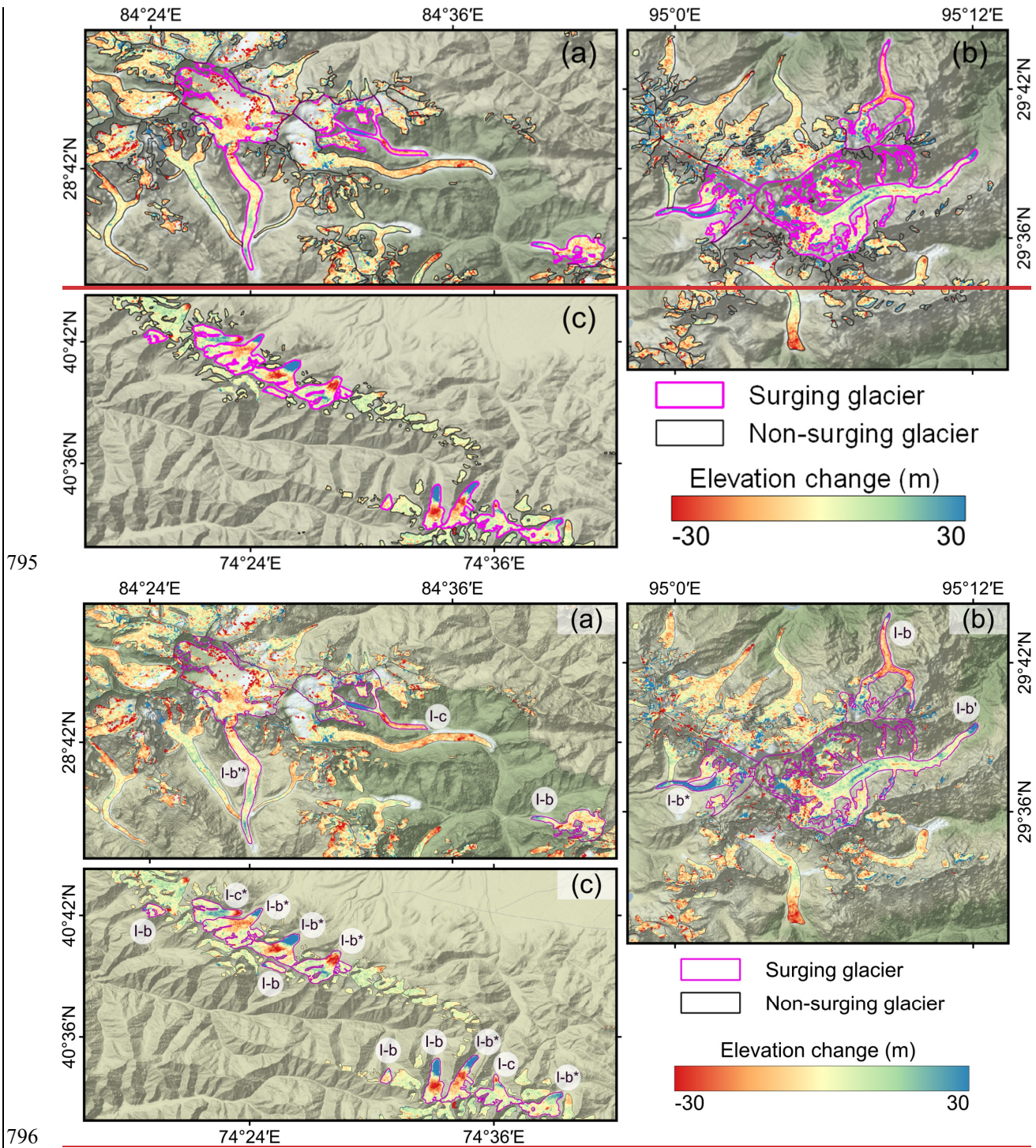
792

793

794

Figure 5: Results of surging glacier identification in (a) the Pamirs (a), (b) Central Tien Shan (b), (c) West Kunlun Shan (c), and (d) Karakoram (d). The background is the shaded relief of SRTM DEM (Source: USGS).





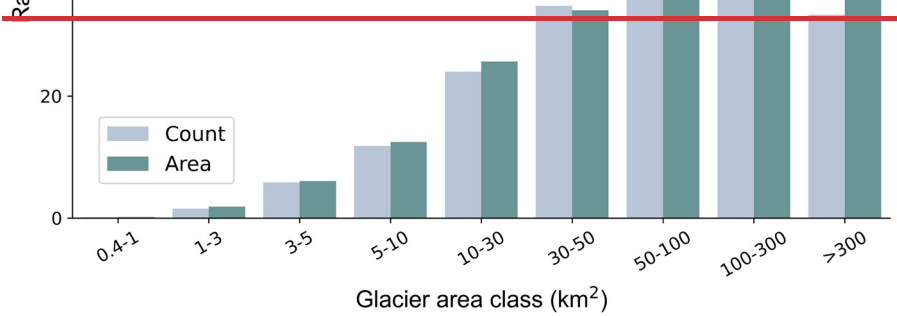
795

796

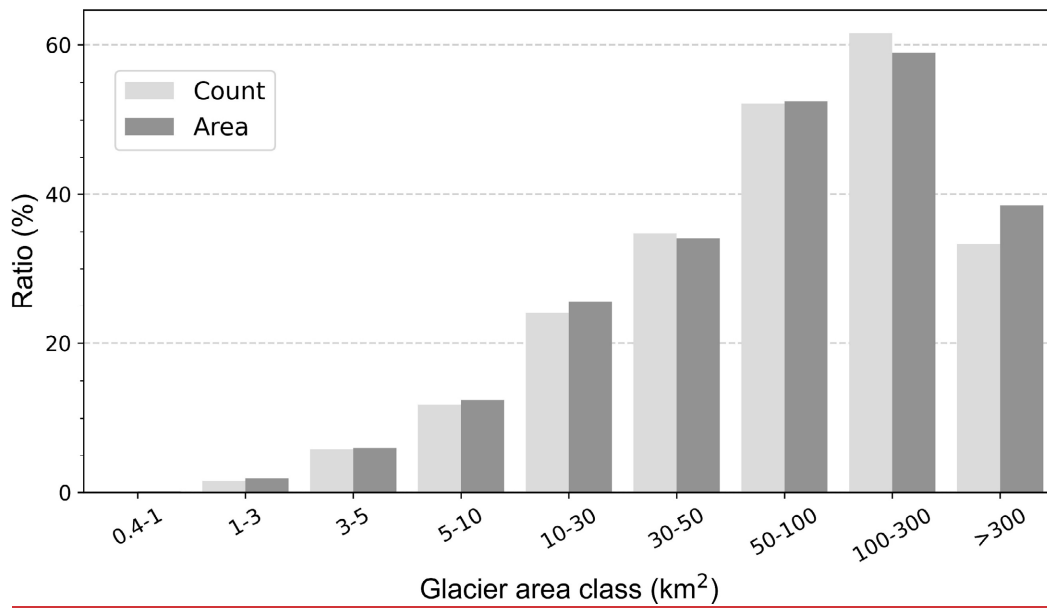
797 **Figure 6: Elevation change map of identified surging glaciers samples in (a) Central Himalaya (1970s-2000), (b) Nyainqentanglha**  
 798 **(1970s-2000), and (c) Northern Western Tien Shan (2000-2020). The labels in panels (a) and (b) represent the identified classes based**  
 799 **on the elevation change pattern. The subscripts “\*” and “’” indicate that the identified class of the glacier is determined by combining**  
 800 **morphological changes, and other elevation change maps, respectively. Background-The background is the shaded relief of SRTM**  
 801 **DEM (Source: USGS). Note that, surging glaciers presented in the figure were identified by combining multi-temporal elevation**  
 802 **change and morphological changes.**

803

Area Class (km <sup>2</sup> )	Total		Surging Glacier		Ratio	
	Count	Area	Count	Area	Count	Area
0.4-1	19428	12215.4	28	20.8	0.14	0.17
1-3	10983	18305.7	169	345.0	1.54	1.88
3-5	2404	9229.4	141	560.3	5.87	6.07
5-10	1650	11370.1	195	1416.4	11.82	12.46
10-30	946	15048.9	227	3861.2	24.00	25.66
30-50	161	5979.1	56	2036.5	34.78	34.06
50-100	92	6337.4	48	3329.2	52.17	52.53
100-300	39	6191.4	24	3651.5	61.54	58.98
>300	6	3466.3	2	1335.6	33.33	38.53



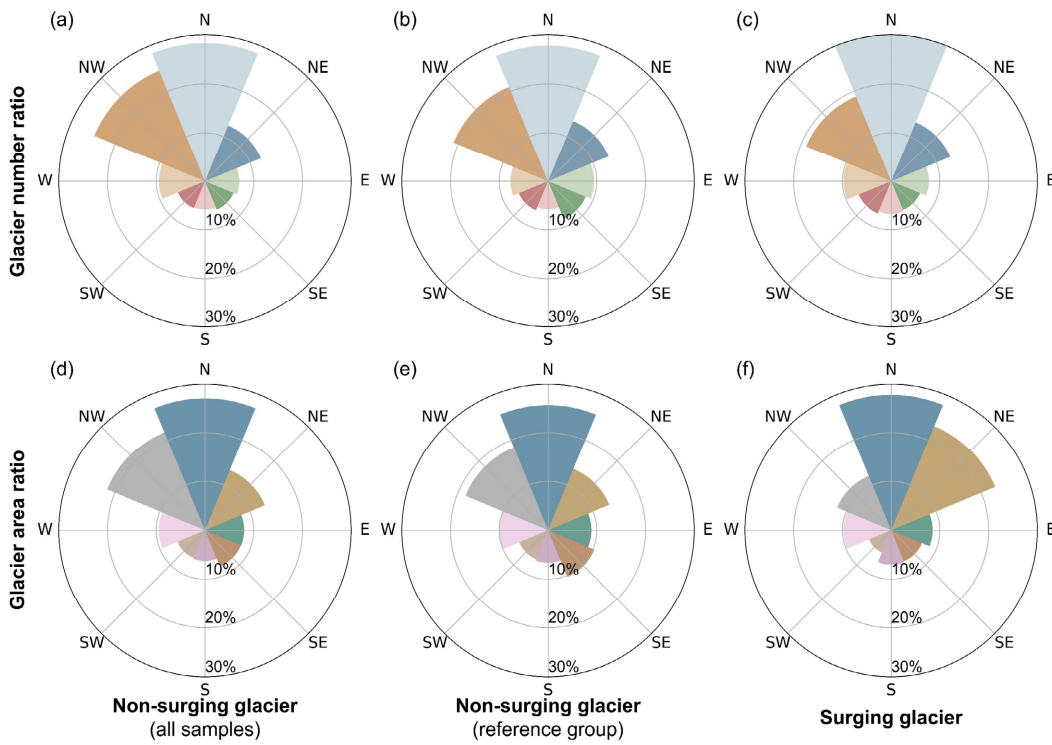
804



805

806

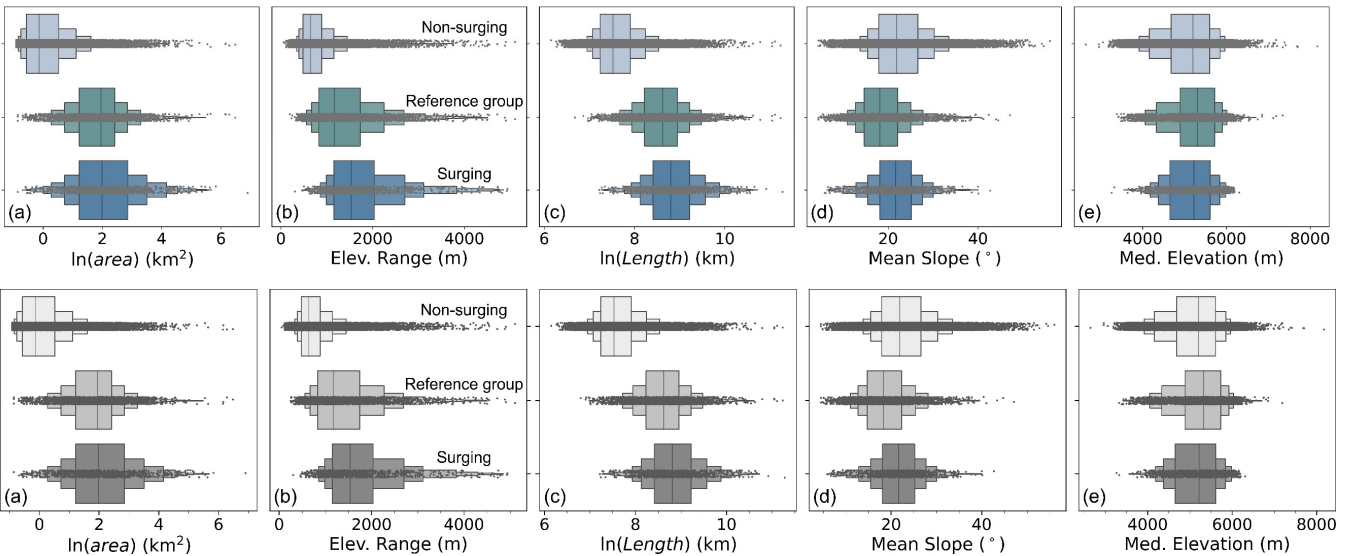
Figure 7: Illustration of the number and area ratios of surging glacier-number and area-ins for different area classes.



807

808 **Figure 8: The distribution of glacier number and area in eight aspect sectors. Left column (a) and (d): distribution of glacier number and area ratio for non-surging glaciers; central column (b) and (e): distribution of glacier number and area ratio for non-surging glaciers in the reference group; right column (c) and (f): distribution of glacier number and area ratio for all surging glaciers. Lower row: glacier area ratio. Left column: distribution of all non-surging glaciers; center column: distribution of non-surging glaciers in the reference group; right column: distribution of surging glacier. Glaciers smaller than 0.4 km<sup>2</sup> were excluded from the non-surging glacier class.**

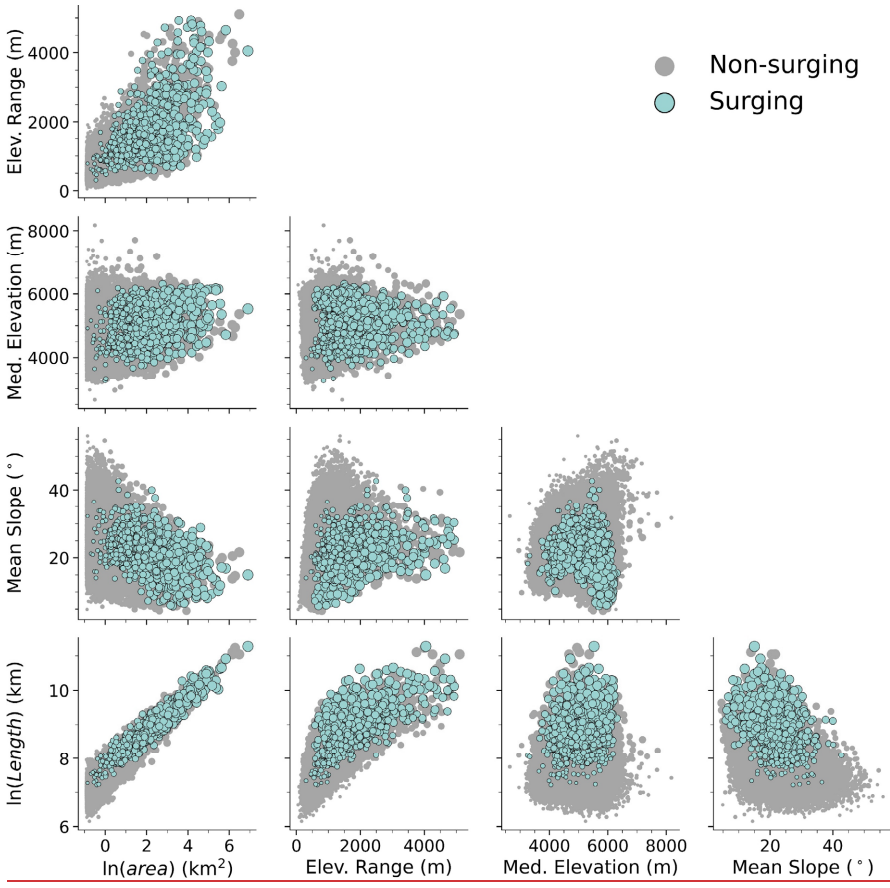
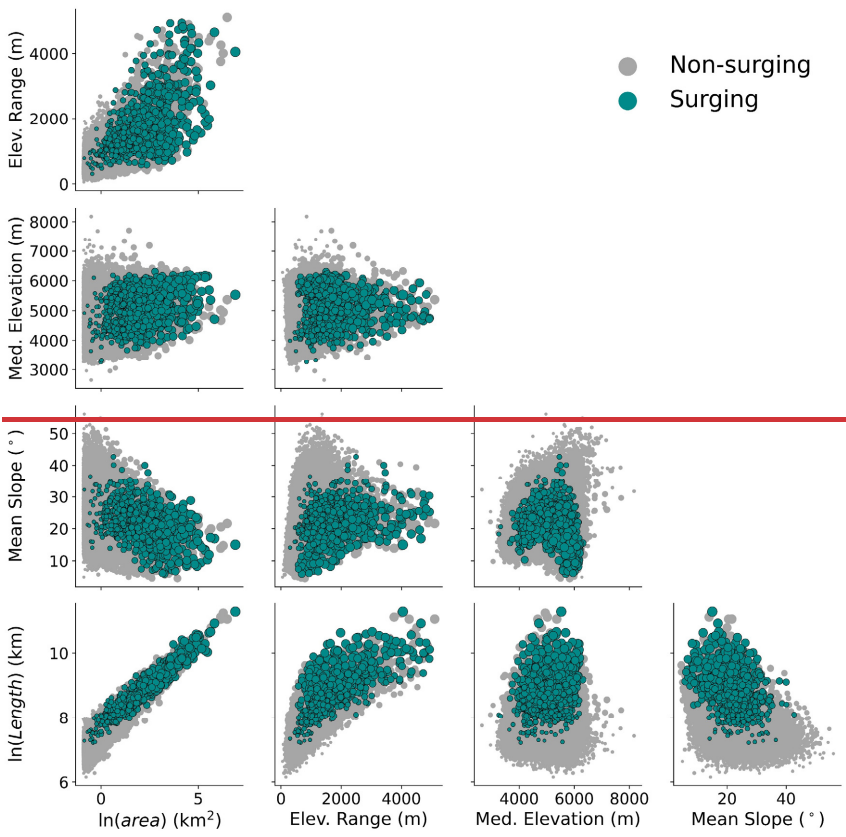
814



815

816 **Figure 9: The comparison between the boxplots of geometric properties of non-surging glaciers (top), non-surging glaciers in the reference group (center), and surging glaciers (bottom). (a) Natural logarithm of area, (b) elevation range, (c) Natural logarithm of length, (d) Mean surface slope, (e) Median elevation. Glaciers smaller than 0.4 km<sup>2</sup> were excluded from the non-surging glacier class.**

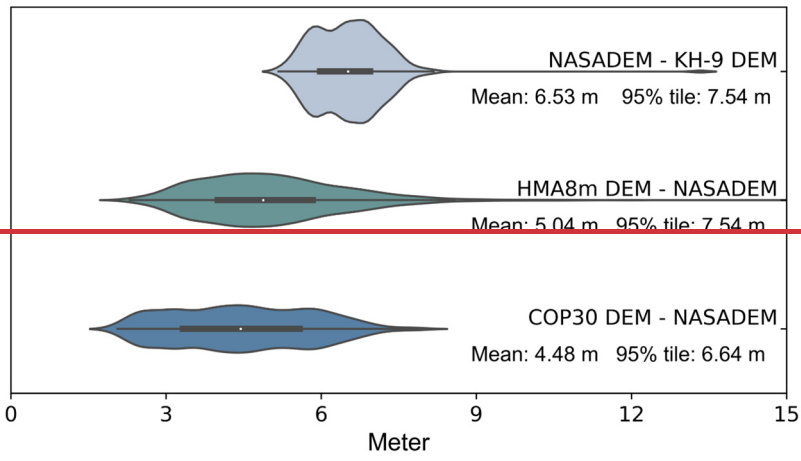




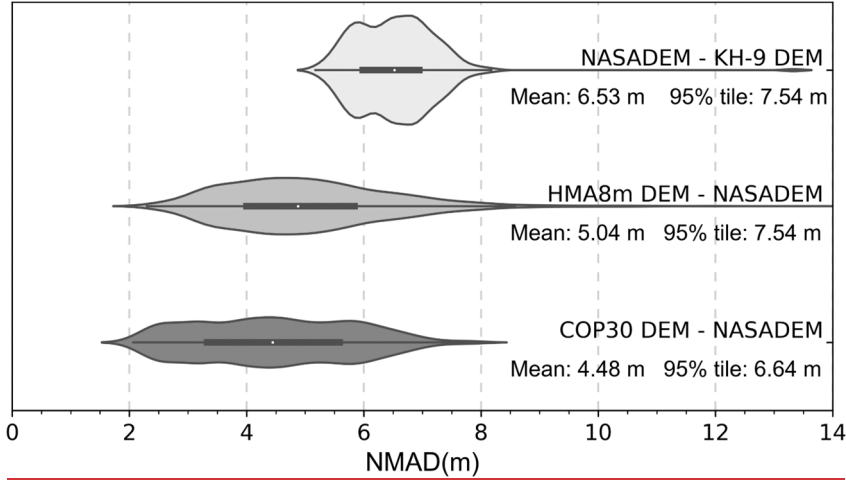
822 **Figure 10: Bivariate scatterplots of geometric properties of non-surg and surging glaciers. The larger dots represent larger**  
 823 **glaciers. Glaciers smaller than 0.4 km<sup>2</sup> were excluded in the non-surg glacier class.**

824

825



826



827

828

829

830

**Figure 11: The distribution of NMAD of elevation change observations in stable areas of all DEM differencing tiles. In each category, the shaded area denotes the density distribution of the NMAD of all DEM differencing tiles. The white dot denotes the median in each group. The thick line represents the interquartile range (IQR, i.e., 75th percentile-25th percentile) in each group. The thin line represents the range between the minimum value (25th percentile - 1.5IQR) and the maximum value (75th percentile + 1.5IQR).**